BROAD LINE RADIO GALAXIES OBSERVED WITH *FERMI*-LAT:
THE ORIGIN OF THE GEV γ-RAY EMISSION

J. Kataoka[1,2], Ł. Stawarz[3,4], Y. Takahashi[1], C. C. Cheung[5], M. Hayashida[6], P. Grandi[7], T. H. Burnett[8], A. Celotti[9], S. J. Fegan[10], P. Fortin[10], K. Maeda[1], T. Nakamori[1], G. B. Taylor[11], G. Tosti[12,13], S. W. Digel[6], W. McConville[14,15], J. Finke[16], F. D'Ammando[17,18]

Draft version July 19, 2011

ABSTRACT

We report on a detailed investigation of the γ-ray emission from 18 broad line radio galaxies (BLRGs) based on two years of *Fermi* Large Area Telescope (LAT) data. We confirm the previously reported detections of 3C 120 and 3C 111 in the GeV photon energy range; a detailed look at the temporal characteristics of the observed γ-ray emission reveals in addition possible flux variability in both sources. No statistically significant γ-ray detection of the other BLRGs was however found in the considered dataset. Though the sample size studied is small, what appears to differentiate 3C 111 and 3C 120 from the BLRGs not yet detected in γ-rays is the particularly strong nuclear radio flux. This finding, together with the indications of the γ-ray flux variability and a number of other arguments presented, indicate that the GeV emission of BLRGs is most likely dominated by the beamed radiation of relativistic jets observed at intermediate viewing angles. In this paper we also analyzed a comparison sample of high accretion-rate Seyfert 1 galaxies, which can be considered radio-quiet counterparts of BLRGs, and found none were detected in γ-rays. A simple phenomenological hybrid model applied for the broad-band emission of the discussed radio-loud and radio-quiet type 1 active galaxies suggests that the relative contribution of the nuclear jets to the accreting matter is $\geq 1\%$ on average for BLRGs, whilst $\leq 0.1\%$ for Seyfert 1 galaxies.

Subject headings: radiation mechanisms: non-thermal — galaxies: active — galaxies: individual (3C 111, 3C 120) — galaxies: jets — gamma rays: galaxies — X-rays: galaxies

1. INTRODUCTION

A long debated problem in our understanding of accreting supermassive black holes (SMBHs) in the Universe is the unification of different types of active galactic nuclei (AGN) in a framework ascribing their observed diversity to a relatively few differing parameters and factors. For example, it has been widely argued that the difference between type 1 and type 2 AGN — i.e., those possessing and lacking broad permitted emission lines in their nuclear spectra, respectively — may be explained by simple geometrical effects involving anisotropic obscuration of the active center viewed at different inclination with respect to the accretion disk axis (Antonucci 1993). The accretion rate was claimed to play a role in this context as well, since 'standard' geometrically-thin optically-thick accretion disks formed at high accretion rates ($> 1\%$ Eddington; Shakura & Sunyaev 1973) on the one hand, and radiatively-inefficient geometrically-thick accretion flows expected to be present at low accretion rates ($< 1\%$ Eddington; Narayan & Yi 1994, 1995; Abramowicz et al. 1995) on the other hand, can account for different emission spectra and power outputs of high- and low-power AGN (see an early discussion on this issue by Fabian & Rees 1995 and Lasota 1996, and the more recent one in Ghisellini et al. 2009). The other relevant parameter may be also the mass of the SMBH itself, which seems to determine some physical differences between Narrow-Line Seyfert 1 galaxies and 'regular' Seyfert 1s (e.g., Pogge 2000; Komossa 2008).

None of the aforementioned factors can, however, account for the dichotomy between radio-loud AGN (which have jets) and radio-quiet AGN (which don't). One may therefore seek the fundamental difference between AGN producing luminous radio-emitting outflows and those lacking such outflows in yet another parameter of the accretion disk/black hole system. One possibility is that, for example, radio-loud AGN harbor rapidly spinning SMBHs with rotational energy extracted electromagnetically via the Blandford & Znajek

[1] Research Institute for Science and Engineering, Waseda University, 3-4-1, Okubo, Shinjuku, Tokyo 169-8555, Japan

[2] email: kataoka.jun@waseda.jp

[3] Institute of Space and Astronautical Science, JAXA, 3-1-1 Yoshinodai, Chuo-ku, Sagamihara, Kanagawa 252-5210, Japan

[4] Astronomical Observatory, Jagiellonian University, 30-244 Kraków, Poland

[5] National Research Council Research Associate, National Academy of Sciences, Washington, DC 20001, resident at Naval Research Laboratory, Washington, DC 20375, USA

[6] W. W. Hansen Experimental Physics Laboratory, Kavli Institute for Particle Astrophysics and Cosmology, Department of Physics and SLAC National Accelerator Laboratory, Stanford University, Stanford, CA 94305, USA

[7] INAF-IASF Bologna, 40129 Bologna, Italy

[8] Department of Physics, University of Washington, Seattle, WA 98195-1560, USA

[9] Scuola Internazionale Superiore di Studi Avanzati (SISSA), 34014 Trieste, Italy

[10] Laboratoire Leprince-Ringuet, École polytechnique, CNRS/IN2P3, Palaiseau, France

[11] University of New Mexico, MSC07 4220, Albuquerque, NM 87131, USA

[12] Istituto Nazionale di Fisica Nucleare, Sezione di Perugia, I-06123 Perugia, Italy

[13] Dipartimento di Fisica, Università degli Studi di Perugia, I-06123 Perugia, Italy

[14] NASA Goddard Space Flight Center, Greenbelt, MD 20771, USA

[15] Department of Physics and Department of Astronomy, University of Maryland, College Park, MD 20742, USA

[16] Space Science Division, Naval Research Laboratory, Washington, DC 20375-5352

[17] IASF Palermo, 90146 Palermo, Italy

[18] INAF-Istituto di Astrofisica Spaziale e Fisica Cosmica, I-00133 Roma, Italy

(1977) mechanism, and converted to the kinetic luminosity of relativistic jets. At the same time, the negligible angular momentum of SMBHs hosted by radio-quiet AGN precludes the formation of such powerful well-collimated outflows. This so-called 'spin paradigm' (Blandford 1990) has recently been claimed to be supported, after some modifications, by several observational findings and theoretical investigations (e.g., Koide et al. 2002; Sikora et al. 2007; Tchekhovskoy et al. 2010, see also in this context Garofalo 2009). Regardless of this debate, the presence of a relativistic jet constitutes a fundamental distinction between various types of AGN, simply because an anisotropic and strongly Doppler-boosted jet emission can dramatically affect the observed properties of a source. In this context, geometrical effects play again a major role. In particular, the total radiative output of those radio-loud AGN which are observed at small viewing angles to the jet axis ('blazars') may be dominated by the broad-band jet emission, while those AGN which are inclined at larger viewing angles (e.g., radio galaxies) may display radiative signatures of both outflowing and accreting matter at comparable levels (see, e.g., Barthel 1989; Urry & Padovani 1995). We note that in addition to such geometrical effects, the age of a radio structure (i.e., the time elapsed after the onset of the jet activity in the nucleus) is yet another factor crucial to understanding unification of radio-loud AGN (see, e.g., O'Dea 1998).

Interestingly, new deep radio surveys indicate that the radio-loudness parameter — which is defined as a ratio of the jet-related radio flux to the disk-related optical flux, and is considered as a proxy for the jet production efficiency[19] — shows a continuous distribution rather than a sharp division between radio-loud and radio-quiet AGN. This applies to AGN hosted by early-type galaxies and accreting at high rates (i.e., quasars), which are typically studied in this context (e.g., White et al. 2000), but holds also when other elliptical-hosted AGN (radio galaxies) spanning a wide range of the accretion rate are taken into account (Sikora et al. 2007). Moreover, unresolved non-thermal radio emission and jet-like structures have been discovered in classes of AGN considered previously as 'radio quiet', i.e., Seyfert galaxies, although the jets in such systems are non-relativistic and weak when compared to the jets found in 'classical' radio galaxies and quasars (e.g., Ulvestad & Wilson 1989; Kukula et al. 1995; Thean et al. 2001; Middelberg et al. 2004, and references therein). The distribution of radio-loudness parameter in Seyferts, which are typically hosted by late-type (disk) galaxies is, however, similarly a continuous function of the accretion rate, as demonstrated first by Ho & Peng (2001) and Ho (2002). Yet, it was pointed out by Sikora et al. (2007) that there is a substantial difference in the distribution of the jet production efficiency between disk-hosted and elliptical-hosted AGN, with Seyfert galaxies being characterized, at any accretion rate, by the radio-loudness parameters orders of magnitudes smaller than the analogous parameters characterizing elliptical-hosted radio galaxies or quasars. Clearly, more studies regarding the jet-disk connection in different types of AGN are needed to understand the jet launching processes and the physics of active SMBHs in general.

[19] More accurately, the radio-loudness parameter depends not only on the total power of a jet relative to the total power of an accreting matter, but also on their respective radiative efficiencies. Only if these radiative efficiencies are not very different between various types of AGN (and various AGN of the same type), the radio-loudness parameter may be considered as a good proxy for the jet production efficiency.

In this context, broad line radio galaxies (BLRGs) seem ideal targets for an in-depth investigation, since this particular class of very radio-loud AGN exhibits both the disk-related ('Seyfert-like') and the jet-related ('blazar-like') radiative signatures in their broad-band spectra. Unlike blazars, the jets in BLRGs are not pointing directly toward the observer, and so the relativistic beaming effects and the related jet dominance are only moderate. Moreover, unlike narrow-line radio galaxies (NRLGs) — which are believed to be intrinsically similar but simply inclined at systematically larger jet viewing angles — BLRGs are not generally obscured by large amounts of dust distributed in torus-like structures around the nucleus, and hence radiative properties of the accretion disks and of the circumnuclear gas can be easily accessed in their case. BLRGs show in particular optical/UV continuum and emission-line characteristics very similar to those of luminous Seyfert galaxies, which indicates high accretion rates and the presence of standard Shakura-Sunyaev disks in both classes of objects. Some fundamental differences in the X-ray spectra between BLRGs and high-accretion-rate Seyferts have been however noted. Specifically, even though the observed X-ray/soft γ-ray emission of BLRGs seem still dominated by the moderately absorbed emission by the accreting plasma (i.e., disks and disk coronae), rather than by the jets, the $1-100$ keV continua of BLRGs are flatter, and their reflection components (as well as the fluorescent Fe Kα lines) weaker than in the case of luminous Seyfert galaxies (e.g., Maraschi et al. 1991; Wozniak et al. 1998; Sambruna et al. 1999, 2002; Eracleous et al. 2000; Zdziarski & Grandi 2001; Ballantyne 2007). Because of such differences, several authors in the past speculated about the non-negligible jet contribution to the X-ray emission of BLRGs, diluting the accretion-related radiative output in the X-ray domain (Wozniak et al. 1998; Eracleous et al. 2000; Grandi et al. 2002). This idea was subsequently examined in various different approaches using most recent broad-band X-ray data obtained with *BeppoSAX* (Grandi et al. 2006; Grandi & Palumbo 2007), *Suzaku* and *Swift* (Kataoka et al. 2007; Sambruna et al. 2009).

Grandi & Palumbo (2007) attempted to disentangle the jet and the disk contributions to the X-ray spectra of three of the brightest BLRGs (the approach first applied to the case of the quasar 3C 273; see Grandi & Palumbo 2004). For simplicity, they assumed that the accretion disks in BLRGs and Seyfert 1 galaxies produce similar emission continua and reprocessing features, and subsequently allowed for a presence of the Doppler-enhanced jet radiation at an arbitrary level. The fits obtained for 3C 120, 3C 390.3 and 3C 382 showed that the data are indeed consistent with a combination of a thermal component (in a first approximation associated with an accretion disk) and a non-thermal component associated with the beamed radiation (due to a jet). Grandi & Palumbo concluded however that jets make only minimal contribution to the X-ray continuum emission of BLRGs, in agreement with the previous findings by Wozniak et al. (1998). More recently, Sambruna et al. (2009) also proposed that BLRGs may be just clustered at one end of the distribution of the X-ray spectral parameters (e.g., photon indices and reflection albedos) characterizing Seyfert galaxies with significant overlap. Interestingly, both Grandi & Palumbo (2007) and Sambruna et al. (2009) suggested that the emission of the underlying jet may instead dominate the radiative output of BLRGs at high energy γ rays, and in particular in the GeV regime.

With the successful launch of the *Fermi* Gamma-ray Space

Telescope, we now have an unprecedented opportunity to study in detail the γ-ray emission from different types of extragalactic sources — not only blazars, but also radio galaxies (Abdo et al. 2009a,c, 2010c,d; Kataoka et al. 2010), and other classes of AGN as well (such as Narrow-Line Seyfert 1 galaxies, for example; Abdo et al. 2009d). During the first 15-month of the *Fermi* mission, 11 non-blazar AGN have been detected in the GeV photon energy range (Abdo et al. 2010a,d) by the *Fermi* Large Area Telescope (LAT; Atwood et al. 2009; Abdo et al. 2010b). This 'misaligned AGN sample' includes seven Faranoff-Riley type I (low-power) radio galaxies, and four Faranoff-Riley type II (high-power, hereafter 'FR II') radio sources consisting of two radio galaxies and two steep spectrum radio quasars. The two luminous radio galaxies detected in γ rays are, in fact, X-ray bright objects classified spectroscopically as BLRGs: 3C 120 (FR I radio morphology), detected for the first time with *Fermi*-LAT, and 3C 111 (FR II radio morphology), whose γ-ray detection was initially reported by EGRET (Hartman et al. 2008) and confirmed by *Fermi*-LAT. None of the X-ray bright Seyfert 1 galaxies appear to be detected in γ rays thus far.

In this paper we report on a detailed investigation of the γ-ray emission from 18 hard X-ray brightest BLRGs, as well as a comparison sample of high accretion-rate Seyfert 1 galaxies selected as their supposed radio-quiet counterparts (in the framework of the AGN unification scheme). Our primary goals are to examine the γ-ray properties of BLRGs as potential 'γ-ray loud' active galactic nuclei, to study the high-energy jet emission in the selected sources, in particular, investigating the relative contributions of the nuclear jet and accretion disk emission in the broad-band spectra of BLRGs. The two years of *Fermi*-LAT exposure provides us with a rather deep all-sky survey reaching the flux limit of typically a few $\times 10^{-12}\,\mathrm{erg\,cm^{-2}\,s^{-1}}$ (95% confidence level) between the observed photon energies 100 MeV and 10 GeV. In §2, we describe the *Fermi*-LAT observations and data reduction procedure. The results of the analysis are given in §3. The discussion and final conclusions are presented in §4. Throughout this paper, a ΛCDM cosmology with $H_0 = 71\,\mathrm{km\,s^{-1}\,Mpc^{-1}}$, $\Omega_\Lambda = 0.73$, and $\Omega_m = 0.27$ is adopted (Komatsu et al 2009).

2. DATA AND DATA ANALYSIS

2.1. *The Sample*

Our sample includes all the BLRGs observed by modern X-ray astronomy satellites (*EXOSAT*, *Ginga*, *ASCA*, *RXTE*, *BeppoSAX*, *Chandra*, *XMM-Newton*, *Suzaku*, *INTEGRAL* and *Swift*), for which data are available at energies above 2 keV. Table 1 presents the list of 18 BLRGs compiled, which also includes for comparison a sample of nine bright Seyfert 1 galaxies chosen from the compilation by Ho & Peng (2001) and Ho (2002), for which the nuclear optical and hard X-ray fluxes match those of the discussed BLRGs. Here we have selected luminous Seyferts 1 with measured radio fluxes (or meaningful upper limits) which, due to their high accretion rates ($> 1\%$ Eddington) and unobscured nuclei, may be considered as radio-quiet analogues of BLRGs (see the discussion in Sikora et al. 2007)[20]. The main difference between the two analyzed classes of sources that should be empha-

sized once more is that Seyferts are radio-quiet and hosted by late-type galaxies, while BLRGs are very radio-loud and elliptical-hosted. The other possibly relevant (but related to the morphologies of host galaxies) difference regards the masses of their SMBHs, $\mathcal{M}_{\mathrm{BH}}$. In particular, nine Seyferts included in our sample are characterized by lower values of black hole masses (median $\approx 10^{6.9}M_\odot$) when compared to the ten BLRGs considered here with $\mathcal{M}_{\mathrm{BH}}$ provided in the literature (median $\approx 10^{8.8}M_\odot$; see Table 1).

The basic information collected from the literature regarding each analyzed source, as listed in Table 1, are (1) IAU coordinates for J2000, (2) source name, (3) redshift z, (4) luminosity distance d_{L}, (5) total 5 GHz flux $[\nu F_\nu]^{\mathrm{tot}}_{5\,\mathrm{GHz}}$ in the cgs units of $\mathrm{erg\,cm^{-2}\,s^{-1}}$, (6) 5 GHz flux of the unresolved nucleus $[\nu F_\nu]^{\mathrm{nuc}}_{5\,\mathrm{GHz}}$, (7) B-band optical flux of the nucleus $[\nu F_\nu]^{\mathrm{nuc}}_{\mathrm{B}}$, (8) X-ray photon index Γ_{X} measured between 2 and 10 keV, (9) average $2-10\,\mathrm{keV}$ flux $[\nu F_\nu]_{2-10\,\mathrm{keV}}$, (10) hard X-ray/soft γ-ray flux $[\nu F_\nu]_{14-195\,\mathrm{keV}}$ detected by *Swift*-BAT at $14-195\,\mathrm{keV}$, (11) black hole mass $\mathcal{M}_{\mathrm{BH}}$, and (12) references. In the case of Seyferts the provided nuclear B-band fluxes (same as in Sikora et al. 2007), which are carefully corrected for the non-negligible starlight contamination, are taken from Ho & Peng (2001) and Ho (2002). In the case of BLRGs, much less severe starlight contamination was taken into account by means of the appropriate correction factors given by Eracleous & Halpern (1994) and Eracleous & Halpern (2003). Also, when a B-band flux was not provided in the literature explicitly, we estimated it from a V-band flux applying a multiplication factor $(\lambda_{\mathrm{V}}/\lambda_{\mathrm{B}})^{1-\alpha_{\mathrm{opt}}}$ with $\lambda_{\mathrm{V}} = 5500\,\text{Å}$, $\lambda_{\mathrm{B}} = 4400\,\text{Å}$, and the assumed optical power-law slope $\alpha_{\mathrm{opt}} = 0.5$. Finally, all the B-band nuclear fluxes listed in column 7 have been corrected for the Galactic extinction available in NED[21]. We note that BLRG 3C 227 has been detected only very recently by *Swift*-BAT at a high significance level (S/N of 4.87; Tueller et al. 2010), but is poorly known at other wavelength. In X-rays, two *Chandra* observations of this object have been conducted so far, as parts of a survey of multiple hot spots in the large-scale structures of nearby radio galaxies. We estimated the $2-10\,\mathrm{keV}$ nuclear flux of 3C 227 from the count rate of *Chandra* ACIS CCD chip given in Hardcastle et al. (2007) using the software PIMMS[22] and assuming the X-ray photon index $\Gamma_{\mathrm{X}} = 1.5$.[23]

We are aware that the compiled sample of BLRGs is by no means statistically complete or unbiased, since the targets were originally selected from independent programs by different observers using different instruments. The final list of objects reflects in fact a bias toward sources which are the brightest in the X-ray domain. Moreover, we are aware that most of the considered objects show flux variability in various energy bands. For example, Turner & Pounds (1989) recorded the minimum X-ray flux of 3C 111 at the level of $1.8 \times 10^{-11}\,\mathrm{erg\,cm^{-2}\,s^{-1}}$, whereas the maximum flux for this source recorded a decade later reached $5.6 \times 10^{-11}\,\mathrm{erg\,cm^{-2}\,s^{-1}}$ in the $2-10\,\mathrm{keV}$ band (Eracleous et al. 2000). Table 1 lists the *average* fluxes measured at different

---

[20] In our sample of Seyfert galaxies we have therefore excluded type $1.5-2$ objects, in order to avoid additional complications related to the absorption of the X-ray emission by the circumnuclear cold gas and dust. We have also
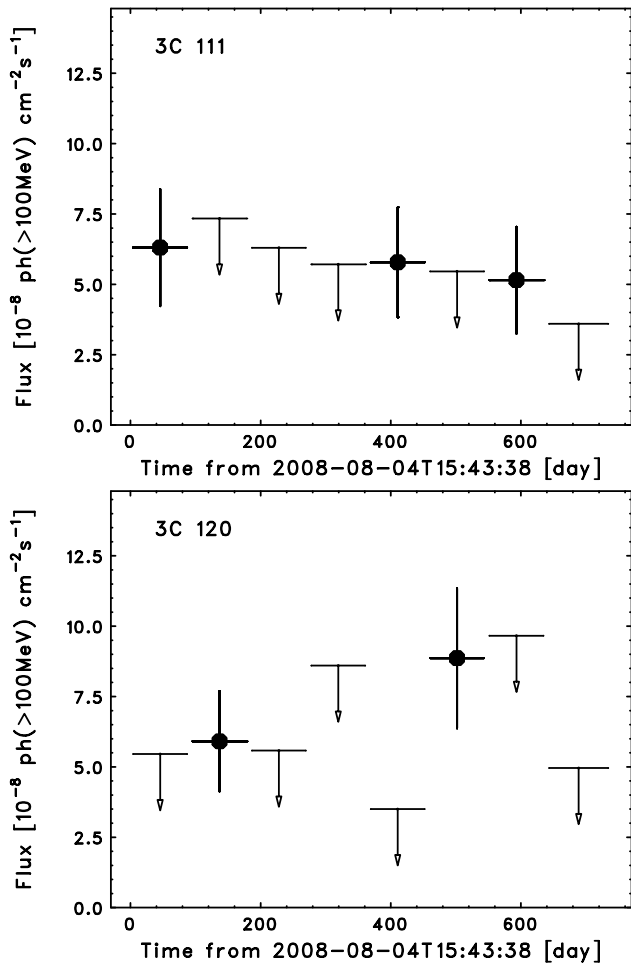
excluded sources such as NGC 4639, which, even though classified as type 1 Seyfert (Sikora et al. 2007), is an example of a low-luminosity AGN accreting at a low rate (Ho et al. 1999).

[21] http://nedwww.ipac.caltech.edu

[22] http://heasarc.nasa.gov/Tools/w3pimm.html

[23] The uncertainty in the assumed X-ray photon index ±0.5 would make only $\simeq 20\%$ difference in the estimated $2-10\,\mathrm{keV}$ flux.

FIG. 1.— Temporal variation of γ-ray flux (> 100 MeV) of 3C 111 (*top*) and 3C 120 (*bottom*) over the period 2008 August–2010 August. The time (in days) is measured from the start of the *Fermi*-LAT observation (2008 August 4, 15:43:38 UT). The fluxes are plotted only when the corresponding TS values exceed 10 for a given time bin, otherwise upper limits are provided.

wavelengths as provided in literature, while at the same time the results discussed later in this paper are not affected by the relatively modest (typically up to a factor of 3) flux variations characterizing X-ray and radio continua of BLRGs[24]. The same caveats apply to the sample of Seyfert galaxies analyzed as it was compiled using even more heterogeneous criteria. Hence it is difficult to identify and to discuss all the possible biases introduced by the applied selection criteria for both samples. Therefore these should be considered simply as lists of prominent (bright) examples of the two discussed classes of AGN.

2.2. *Fermi-LAT Observations and Data Analysis*

The LAT instrument onboard *Fermi* is described in detail in Atwood et al. (2009) and references therein. It is characterized by a larger effective area ($\sim$8,000 cm^2 on axis at 1 GeV for the event class considered here), a wider energy coverage (from $\sim$20 MeV to $>$300 GeV), and an improved angular resolution when compared to the previous γ-ray missions. The

68% containment angles of the reconstructed incoming photon direction are approximated as $\theta_{68} \simeq 0°.8\,(\varepsilon_\gamma/\mathrm{GeV})^{-0.8}$ below 10 GeV. During the first two years of *Fermi*-LAT operation, most of the telescope's time was dedicated to observing in a 'survey mode,' in which the instrument points away from the Earth and nominally rocks the spacecraft axis north and south from the orbital plane to enable monitoring of the entire sky on a time scale shorter than a day. In particular, the whole sky is surveyed every $\sim$ 3 hours (2 orbits).

The dataset used here comprises all the scientific data obtained between August 4, 2008 and August 4, 2010. This time interval runs from Mission Elapsed Time (MET) 239557414 to 302630530, which is consistent with the observation period for the Second *Fermi*-LAT Catalog (2FGL) selection (The Fermi-LAT collaboration 2011, in prep). We have applied the zenith angle cut of $105°$ to eliminate photons from the Earth's limb. We use events from the "Diffuse" class (Atwood et al. 2009), i.e., the events that have the high probability of being photons. In the analysis presented here, we set the lower and higher energy bounds at 200 MeV and 100 GeV, respectively. The choice of a lower energy bound at 200 MeV is conservative but reduces significantly systematic errors. Science Tools[25] version V9R15P2 and Instrumental Response Functions (IRFs) P6_V3_DIFFUSE were used throughout the analysis.

In order to study the average spectrum of each selected target, we use the standard unbinned maximum-likelihood spectral estimator (Mattox et al. 1996) provided with the LAT science tool GTLIKE. It allows us to fit the data to a source model, along with the models for the uniform extragalactic and structured Galactic backgrounds[26]. The Galactic diffuse emission model and the isotropic spectral model used here were developed by the *Fermi*-LAT team as refinements of the publicly released models; this choice does not affect significantly the results for the candidate sources considered, which are all located outside the Galactic plane except for 3C 111[27]. Much more crucial is a careful selection of source regions, especially for relatively faint objects. The model for which we calculate the likelihood is a combination of point-like and diffuse sources for a region of interest (ROI) with the radius of $r = 8°$ centered on the target under consideration[28]. For all the BLRGs and Seyferts listed in Table 1, we first assume a point-like source with a power-law spectrum at the position of each target, and fix the γ-ray photon index as $\Gamma_\gamma = 2.5$. Additional sources from the 1st *Fermi*-LAT Catalog (1FGL; Abdo et al. 2010b) and from the internal LAT collaboration catalog produced using 18 months of data are included in the model of each ROI. Next, using the GTLIKE tool, we find the best-fit parameters for each source and evaluate the significance of the detection given by the test statistic, $\mathrm{TS} = 2\Delta \log(\mathrm{likelihood})$ between the models with and without a source. For sources which are detected above a certain significance threshold ($\mathrm{TS} \geq 25$, corresponding to $\geq 5\sigma$ detections), we retry the GTLIKE fit assuming power-law spectra ($F = K\,E^{-\Gamma_\gamma}$) with *both* parameters (normalization, K and

---

[24] In order to illustrate possible effects caused by the temporal variability of the analyzed sources, in the spectral energy distributions shown in Figures 3, 8 and 9 below we have provided both the minimum and maximum X-ray fluxes whenever available in the literature.

[25] http://fermi.gsfc.nasa.gov/ssc/data/analysis/documentation
[26] http://fermi.gsfc.nasa.gov/ssc/data/access/lat/BackgroundM
[27] With Galactic coordinates ($l = 161°.68$, $b = -8°.82$), 3C 111 is located behind a large molecular cloud complex in Taurus (cf., Dame et al. 2001, Fig. 2 therein), thus requires more care in the analysis due to the expected contamination from Galactic diffuse emission.
[28] See, in this context, Abdo et al. (2009a) for a detailed investigation of changing the radius of ROI from $8°$ to $20°$, and the arguments given for using $r = 8°$ to minimize the contamination from the Galactic diffuse emission.
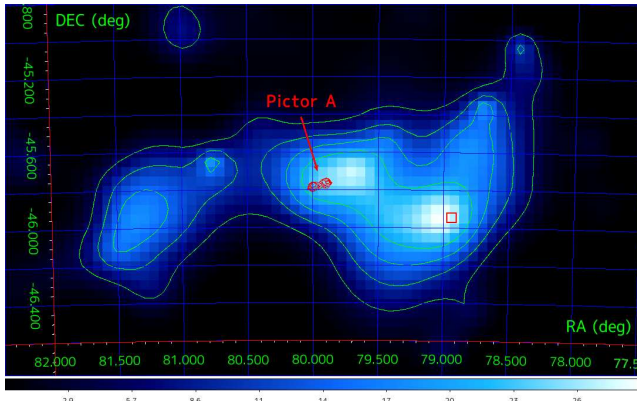
FIG. 2.— *Fermi*-LAT TS map (>200 MeV) centered on Pictor A, show-ing the presence of multiple γ-ray peaks in the field. Contamination from nearby sources are modeled as part of the background that also includes Galactic/extragalactic diffuse γ-ray emission. The *green* contours corre-spond to TS values of 5, 10, 15, and 20, while the *red* contours indicate 1.4 GHz radio emission from Pictor A (Perley et al. 1997). The position of a blazar, BZQJ0515-4556, is also shown as *red box*. The peak near the center of the map (TS = 20) is almost exactly coincident with the position of Pictor A. The TS peaks associated with Pictor A and with BZQ J0515−4556 are only marginally resolved. The TS value quoted here and in Table 2 for Pic-tor A was evaluated using a source model that included point sources at the position of BZQ J0515−4556 and at R.A. = 81.35 deg, Dec. = −45.78 deg.

photon index, Γ_γ) set free, and then calculate the errors on the fluxes and photon indices. For the remaining BLRGs and Seyferts, which are detected in the analyzed dataset below the threshold (TS < 25), we simply provide upper limits on the fluxes for the fixed $\Gamma_\gamma = 2.5$.

3. RESULTS

Table 2 summarizes the results of the *Fermi*-LAT data anal-ysis of the 18 BLRGs and 9 Seyfert galaxies. For each source considered, Table 2 provides (1) name, (2) statistical signif-icance TS of the *Fermi*-LAT detection, (3) γ-ray photon in-dex Γ_γ evaluated for the photon energy range $0.1 - 10\,\mathrm{GeV}$, (4) the integrated photon flux above 100 MeV, $F_{>0.1\,\mathrm{GeV}}$, (5) γ-ray flux $[\nu F_\nu]_{0.1-10\,\mathrm{GeV}}$, (6) the corresponding γ-ray lumi-nosity $L_\gamma = 4\pi d_\mathrm{L}^2 [\nu F_\nu]_{0.1-10\,\mathrm{GeV}}$, (7) total accretion-related luminosity L_acc derived from the spectral fitting as described below, and (8) 'mixing' parameter η discussed in the next sec-tion. Only two BLRGs (3C 111 and 3C 120) are detected at sufficiently high significance levels, i.e., TS ≥ 25, in the ac-cumulated two-year *Fermi*-LAT dataset. For these, the γ-ray fluxes and luminosities are evaluated straightforwardly[29]. For the targets detected at lower significance levels, TS < 25, the corresponding 95% confidence level flux upper limits are calculated using the dedicated software UPPERLIMIT.PY.

For 3C 120, the results presented here are consistent with those reported in Abdo et al. (2010d), but with reduced un-certainties in the flux and photon index due to the improved photon statistics based on the two-year accumulation of the *Fermi*-LAT data. We note however that the TS value in-creased only slightly between the 15-month and 24-month *Fermi*-LAT datasets (cf., TS = 34 found here vs. TS = 32 re-ported in Abdo et al. 2010d). In contrast, the flux and photon index uncertainties increased in the case of 3C 111, and the corresponding TS value decreased between the 15-month and

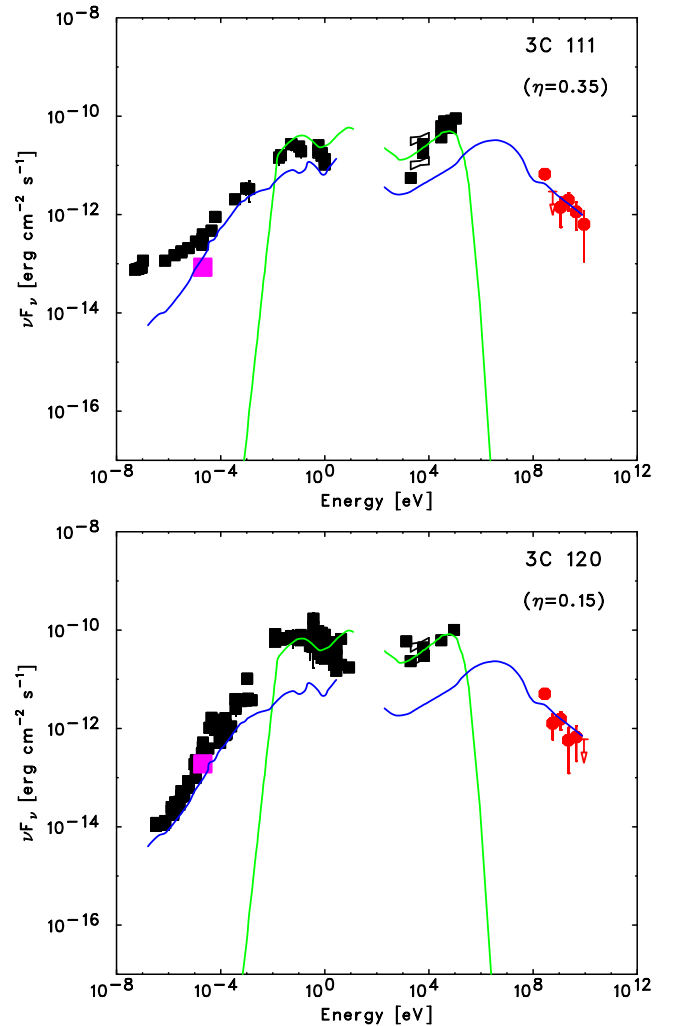

FIG. 3.— Broad-band SEDs of the two BLRGs detected at high significance by *Fermi*-LAT (3C 111 and 3C 120). *Fermi*-LAT data are indicated by red cir-cles. Black squares represent the historical data from NED. Magenta squares denote the 5 GHz radio fluxes of the unresolved nuclei (if available). The green curves correspond to the template of the accretion-related Seyfert-type emission (from Koratkar & Blaes 1999), matched to the infrared–to–X-ray continuum of each source. The blue curves correspond to the broad-band spectrum of the quasar 3C 273 (from Soldi et al. 2008), used here as a tem-plate of the jet-related emission and scaled to match the radio fluxes for each source. The mixing parameter η for the phenomenological hybrid model dis-cussed in § 4 is given in each panel.

24-month *Fermi*-LAT datasets (cf. TS = 31 found here vs. TS = 34 reported in Abdo et al. 2010d). The reason for this behavior is twofold. First, the likelihood analysis was lim-ited here to the photon energy range $0.2 - 100\,\mathrm{GeV}$, whereas the energy range $0.1 - 100\,\mathrm{GeV}$ was adopted in Abdo et al. (2010d). The difference in energy selection is relevant since 3C 111 is located at a relatively low Galactic latitude (see footnote 27), and as such is heavily affected by the contam-ination from the Galactic diffuse emission especially below $200\,\mathrm{MeV}$ [30]. If we *lower* the photon energy threshold of the likelihood analysis to 100 MeV, the significance of the 3C 111

---

[29] Since the likelihood analysis was limited to the photon energy range $0.2 - 100\,\mathrm{GeV}$, all the flux values and the corresponding luminosities are extrapolated down to 100 MeV with a given photon index. This choice is dictated solely by the *convention* typically followed by the γ-ray community.

[30] Accordingly, in the 1FGL catalog (Abdo et al. 2010b, table 4 therein), the source fit of 1FGL J0419.0+3811 was flagged as being sensitive to changes in the diffuse Galactic emission model (flux and spectral index could change by more than 3σ). However, upon close inspection of the dust col-umn density $E(B - V)$ and W(CO) maps (Schlegel et al. 1998; Dame et al. 2001), we estimated that the possible enhancement of γ-ray emission at the
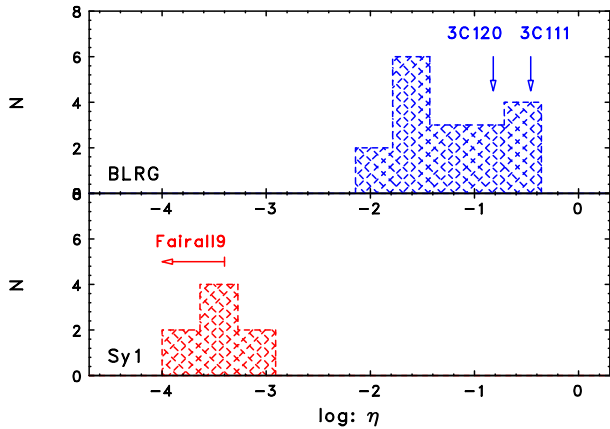
FIG. 4.— Distribution of a mixing parameter η for BLRGs (*top* panel; blue histogram) and Seyferts (*bottom* panel; red histogram). The values characterizing the two detected sources (3C 111 and 3C 120) are indicated by the arrows in the top panel. In the case of Fairall 9, which is not detected in radio, an upper limit for the η parameter is given in the *bottom* panel.

detection in the 24-month data increases (TS = 59), as expected. Second, as noted in Abdo et al. (2010d), the considered galaxy seemed variable in the GeV range, being in particular brighter at the very beginning of *Fermi*-LAT observations. Here we investigate this issue in more detail, showing in Figure 1 (*top* panel) the temporal variations of the γ-ray flux of 3C 111 above 100 MeV using the two-year accumulation of the *Fermi*-LAT data binned in the 3-month-long periods. The fluxes are plotted only when the detection significance reached TS > 10 in a given time bin; in the case of 3C 111 such a criterion was fulfilled only in three time intervals out of 8 total. Even lower γ-ray duty cycle emerges from the 3C 120 lightcurve, as also shown in Figure 1 (*bottom* panel). All in all, we conclude that both BLRGs detected by *Fermi*-LAT are variable in the GeV photon energy range, even though the significance of the variability can hardly be evaluated due to the insufficient photon statistics. A dedicated analysis of all EGRET data also indicated plausible variability of the MeV/GeV emission in 3C 111 (Hartman et al. 2008). Note also that over the past two years both BLRGs have declined in flux by ~30% at centimeter wavelengths as observed by the Univ. of Michigan Radio Astronomy Observatory[31]. In 3C 111 specifically, a bright sub-mm (230 GHz) flare was observed toward the end of 2008 (Chatterjee et al. 2011), co-inciding with the period of the initial ~0.5 years of LAT observations, with a subsequent decline in the sub-mm flux over the next ~1.5 years.

At this point let us also comment on the particular case of Pictor A galaxy, for which a relatively high TS value has been found (see Table 2), yet below the critical value of 25 required for claiming the detection. In fact, in the analysis procedure described above (i.e., assuming a *single* point-like source at the position of the galaxy, R.A. = $79°.957$ and Dec = $-45°.779$), one can find formally TS = 45 for Pictor A. However, a close inspection of the spatial distribution of TS for the whole source region (hereafter the 'TS map') reveals a rather complex structure elongated substantially in the RA direction, which is inconsistent with a single point

position of 3C 111 due to additional column density from dark gas or a somewhat larger emissivity may account for at most, ~10 % of the γ-ray flux listed in Table 2.

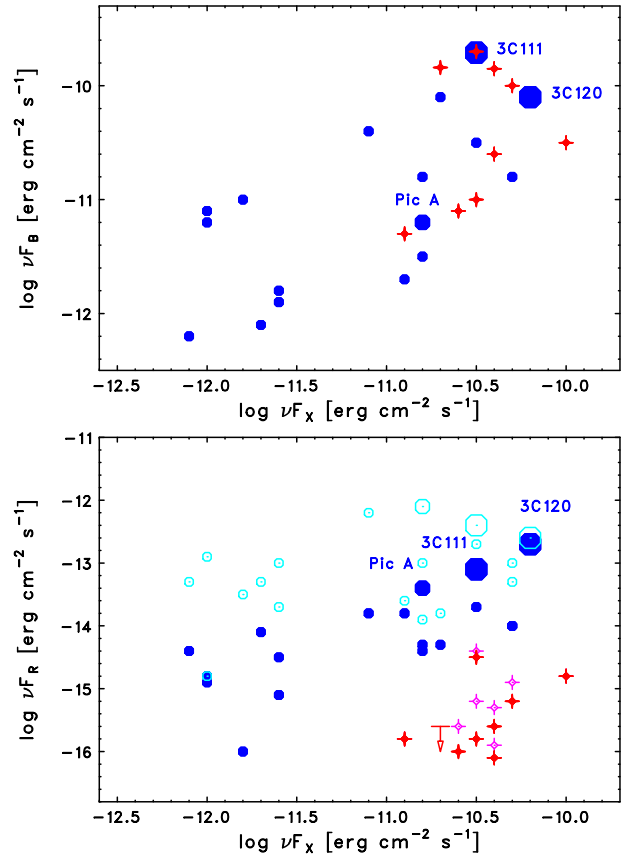[31] http://www.astro.lsa.umich.edu/obs/radiotel/umrao.php

FIG. 5.— *Top* panel: the optical (*B*-band) versus X-ray (2 − 10 keV) fluxes for all the sources included in the sample, with BLRGs denoted by blue filled circles and Seyferts by red crosses. *Bottom* panel: the radio (5 GHz) versus X-ray (2 − 10 keV) fluxes. Here BLRGs are plotted as blue filled cycles when nuclear radio fluxes are used, and as cyan open circles when total radio fluxes are considered. Similarly, Seyfert 1 galaxies are plotted as red crosses when nuclear radio fluxes are used, and as magenta crosses when total radio fluxes are considered. An upper limit is given for Fairall 9. In both panels, large symbols indicate the two objects detected by *Fermi*-LAT (3C 111 and 3C 120), while the medium-size symbols represent Pictor A galaxy which, even though not formally detected, is characterized by the third-highest TS in the analyzed two-year *Fermi*-LAT dataset.

source. Figure 2 shows TS map thus obtained, where contamination from nearby sources (listed in the 1FGL and in the internal LAT collaboration catalog using 18 months of data) are modeled as part of the background that also includes Galactic/extragalactic diffuse γ-ray emission. This suggests a presence of multiple γ-ray sources in the field. More exactly, in a careful examination of the TS map we found three emission peaks (each about a degree apart), one of which coincides almost exactly with the position of Pictor A, being characterized by TS = 20. Also, one of the other two emission peaks located at R.A. = $79°.09$, Dec = $-46°.08$ is positionally coincident with a blazar BZQ J0515−4556 (R.A. = $78°.94$, Dec = $-45°.95$) with a TS value of 19. The last peak seen to the east of Pictor A is less prominent (TS value of 11) and located at R.A. = $81°.35$, Dec = $-45°.78$. Sources at the positions of the two TS peaks just mentioned were included in the model when the TS for Pictor A listed in Table 2 was evaluated. Hence, one may conclude that there are some indications for the GeV emission of Pictor A galaxy close to the upper limits provided in Table 2, and that the formal detection of this object by *Fermi*-LAT in the near future is quite likely.

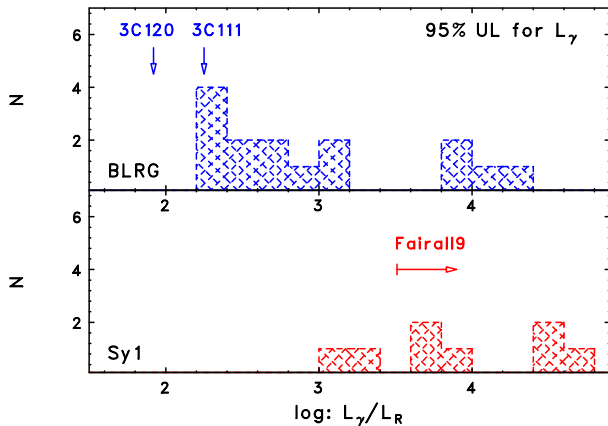No statistically significant detection of any Seyfert 1 galaxy

FIG. 6.— Upper limits for the ratio of the monochromatic γ-ray and nuclear radio luminosities for BLRGs (*top* panel; blue histogram) and Seyferts (*bottom* panel; red histogram) that are not detected by *Fermi*-LAT . The values characterizing the two detected sources (3C 111 and 3C 120) are indicated by the arrows in the top panel. Since Fairall 9 is not detected in radio, a lower limit is given in the *bottom* panel.

analyzed was found in the 24-month *Fermi*-LAT dataset. Interestingly, IC 4329A shows a relatively high TS value of 15 (see Table 2), but this could be due to a contamination from a nearby source. This nearby source was found only recently, and has been associated tentatively with a blazar in the 2FGL catalog (The Fermi-LAT collaboration 2011, in preparation). Nevertheless, the provided upper limits for the γ-ray emission of the considered sample of Seyferts — typically at the flux level of a few $\times 10^{-12}$ erg cm^{-2} s^{-1} between 0.1 and 10 GeV, depending on the degree of the contamination from the Galactic diffuse emission and on the presence of nearby bright γ-ray sources — provide interesting constraints as discussed below.

4. DISCUSSION AND CONCLUSIONS

The analysis of the two year *Fermi*-LAT data for the selected 18 X-ray–bright BLRGs confirmed the previously reported detections of the two sources (3C 120 and 3C 111), at the significance levels not much different between the 15-month and 24-month datasets. This may indicate that the observed γ-ray emission is variable on months to year timescales, with a relatively low duty cycle, as revealed by a closer inspection of the corresponding lightcurves (Figure 1). In fact, the > 100 MeV γ-ray flux of 3C 111 observed with *Fermi*-LAT is $(3.5 \pm 1.2) \times 10^{-8}$ ph cm^{-2} s^{-1}, which is about $\sim 20\times$ smaller than the maximum recorded by EGRET in the same energy range (64×10^{-8} ph cm^{-2} s^{-1}, Hartman et al. 2008), thus suggesting significant variability in the decade timescale between the EGRET and *Fermi*-LAT observations. Moreover, we found some hints for γ-ray emission from Pictor A (TS = 20), even though we cannot claim a formal detection at the moment. These results suggest that other BLRGs could be promising candidates for *Fermi*-LAT detections in the near future, and that BLRGs in general could potentially constitute a class of γ-ray loud AGN. Such a statement is however difficult to quantify, because of the aforementioned variability of the GeV fluxes from 3C 120 and 3C 111 (assuming that both galaxies are representative for the whole class). On the other hand, the observed flux changes from these two detected galaxies imply that, in analogy with blazar sources, the GeV continua of BLRGs are produced predominantly in the inner parts of their nuclear outflows (jets on scales less than tens or hundreds of parsecs). In fact, as

noted in the previous sections, several authors have previously suggested that the GeV radiation from BLRGs, if detected, should most likely be due to non-thermal and beamed blazar-type emission, but only observed at intermediate inclinations (jet viewing angles, say, $10° \lesssim \theta_j \lesssim 30°$, versus $\theta_j \lesssim 10°$ expected for blazars; see Grandi & Palumbo 2007; Sambruna et al. 2009). Interestingly, unlike in the luminous blazars, the X-ray/soft γ-ray spectra of BLRGs (up to the observed photon energies of ~ 100 keV) have been argued to be dominated by the thermal radiation of the accreting matter (Wozniak et al. 1998; Sambruna et al. 1999; Eracleous et al. 2000; Zdziarski & Grandi 2001), with only little (if any) jet contribution (Grandi & Palumbo 2007; Kataoka et al. 2007; Sambruna et al. 2009). Hence it is clear that BLRGs are truly ideal targets for investigating the AGN jet-disk connection in the X-ray/γ-ray regime. Here we present a few considerations regarding this issue.

Figure 3 presents spectral energy distributions (SEDs) of the two aforementioned γ-ray–detected BLRGs; the SEDs of all the remaining objects, for which only the upper limits in the *Fermi*-LAT range were derived, are given in Figures 8 and 9 further below (see Appendix A). In the figures, the *Fermi*-LAT data are indicated by red circles (or arrows), black squares represent the historical data from NED, while the magenta squares show the 5 GHz radio fluxes of the unresolved nuclei. Even though the broad-band spectra vary to some degree between 3C 120 and 3C 111 (e.g., with respect to the ratio between the total and the nuclear radio luminosities), one can gauge the main similarities and differences between the BLRG-type and Seyfert-type SEDs. In particular, while the infrared–to–hard X-ray continua of the two BLRGs are very similar to the one characterizing Seyfert galaxies considered here, the former objects are significantly brighter than the representative Seyfert in the radio and γ-ray domains. Such a dramatic difference in the radio loudness is related to the presence of a relativistic jet, as discussed above, and here we suggest that same is true regarding the γ-ray loudness. To investigate it further more quantitatively (yet still illustrative), we consider a simple phenomenological 'hybrid' model for the broad-band emission of a type 1 AGN, consisting of individual thermal and the non-thermal emission components (the approach analogous to the one adopted in Grandi & Palumbo 2004, 2007). The thermal component, related to the radiative output of the accreting and circumnuclear matter (accretion disk, disk corona, dusty torus), is approximated here by the template Seyfert spectrum given by Koratkar & Blaes (1999). For the non-thermal broad-band emission component of the nuclear (blazar-type) relativistic jet observed at intermediate viewing angles, we use the well-constrained SED of the radio-loud quasar 3C 273 (from Soldi et al. 2008) as a template[32]. Both templates, plotted in Figure 3 (as well as in Figures 8 and 9) as green and blue curves, respectively, are rescaled to match the data points for the analyzed sources. If the *Fermi*-

---

[32] It should be emphasized here that the observed multiwavelength emission of 3C 273 is *not purely non-thermal* in origin. For example, Grandi & Palumbo (2004) estimated that about a quarter to half of the $2 - 10$ keV flux of this source could be due to the accreting matter, and not due to the jet. However, the "big blue bump" is clearly visible in the overall SED of the quasar around UV/soft X-ray frequencies is almost certainly due to the accretion disk. Nevertheless, the broad-band spectrum of 3C 273 is the best sampled (and best understood) spectrum of a quasar dominated in radio and in γ rays by the moderately-beamed emission of a powerful jet observed at intermediate viewing angles ($\theta_j \sim 10°$; see Courvoisier 1998, and references therein). As such, it can indeed be consider as the best available template for the jet-related emission of BLRGs.
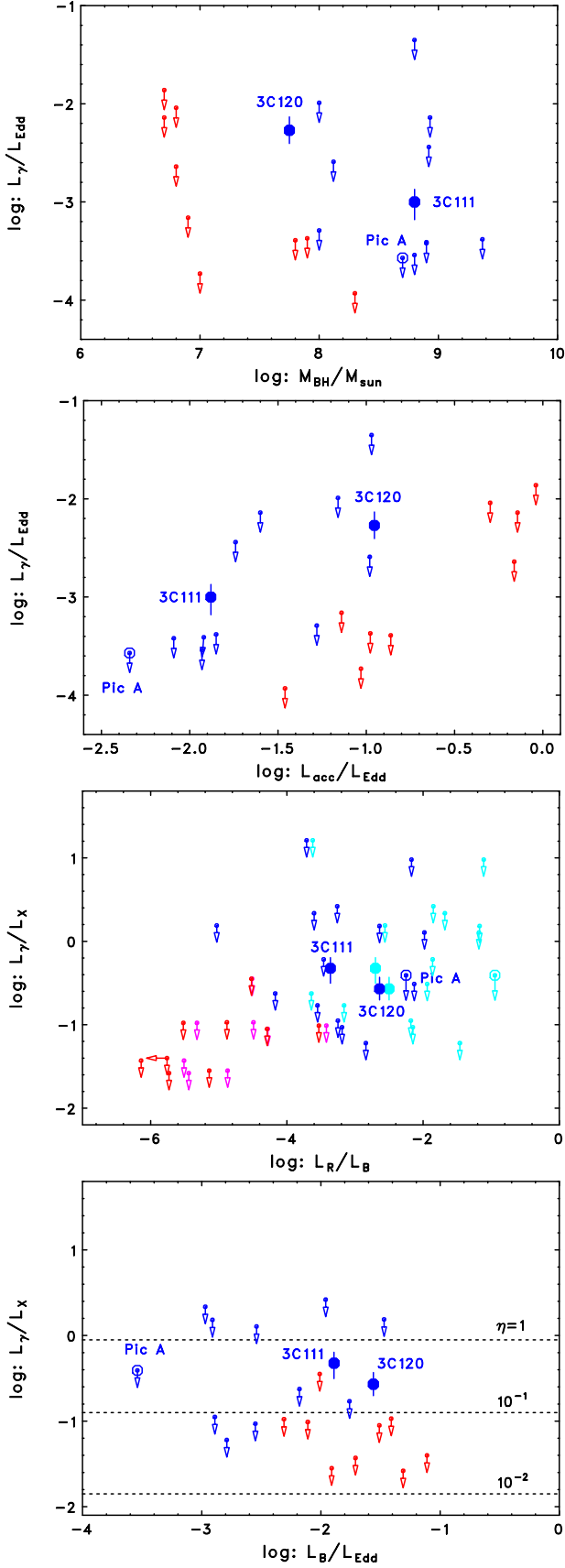
LAT did not detect the source and only upper limits on γ-ray flux were derived, its non-thermal component is entirely determined by the 5 GHz nuclear flux (in this context, see Table 3 of Ghisellini et al. (2005), who predicted γ-ray fluxes of 3CR FR I radio galaxies from 5 GHz core fluxes). This allows us to approximate the relative contribution of the non-thermal and thermal emission components to the observed SED of each object, in terms of a 'mixing' parameter (η). Under the adopted definition, this parameter increases with the increasing contribution of the jet-like component, and equals unity when both the 3C 273 and the Seyfert template spectra provide comparable contributions to the observed UV flux of a source. Note that the direct radiation of the standard (Shakura-Sunyaev) AGN accretion disk is expected to peak in the UV regime (photon energies $\sim 10\,\mathrm{eV}$).

Obviously, the adopted model is an oversimplification of a realistic situation, as it ignores several complications which may be potentially relevant. For example, it is at some level questionable to use the broad-band spectrum of the radio-loud quasar 3C 273 as a template for the jet-related emission of Seyfert galaxies in general. Moreover, possible (or even likely) temporal variability of each source considered, as well as the *ad hoc* adopted procedure of matching the assumed templates to the collected data points, precludes any robust statistical analysis (e.g., χ^2 fitting) which would allow for the values and errors of the η parameter to be determined more accurately. Nevertheless, it is worth noting that this simple model seems to match the SEDs of the two BLRGs well from radio to γ-ray frequencies, and that in both cases the emerging values of the η parameter are similar ($\simeq 0.15 - 0.35$), being in addition consistent with the ones following from the analysis by Grandi & Palumbo (2007). Importantly, the model when applied to the other BLRGs analyzed here returns similar values for the η parameter at the level of few tens of percent at most (as determined by the nuclear radio fluxes), without violating the *Fermi*-LAT upper limits (see column 8 in Table 2 and the SEDs presented in Figures 8). Figure 4 presents the distribution of the mixing parameter η emerging from the SED matching. This distribution suggests that, even though the particular frequency ranges may be dominated by one of the two main emission components, the *total* observed luminosities of the nuclear jets in BLRGs constitute on average not less than 1% of the accretion-related luminosities (median $\eta \approx 0.10$), and that in the case of a few particular objects the jet–to–disk luminosity ratio may even approach unity. An interesting implication of the above statement, strengthened thanks to the inclusion of the *Fermi*-LAT data in our modeling, is that one should expect a non-negligible non-thermal emission component in BLRGs in the MeV energy range, constituting as much as $\sim 1\% - 10\%$ of the total power emitted in the hard X-ray domain. If correct, this may be of importance for understanding the recently debated origin of the extragalactic MeV background (see the discussions in Inoue et al. 2008; Ajello et al. 2009). On the other hand, the contribution of the jet emission to the total radiative output of the Seyfert 1 galaxies are in general very small (median $\eta \approx 5 \times 10^{-4}$; see Figure 4 and the SEDs shown in Figure 9).

To investigate further the collected dataset, we plot the optical $[\nu F_\nu]_\mathrm{B}$ versus X-ray $[\nu F_\nu]_{2-10\,\mathrm{keV}}$ fluxes for all the sources included in the sample in Figure 5 (the *top* panel), with BLRGs denoted by blue filled circles and Seyferts by red crosses. The *bottom* panel of Figure 4 presents instead the radio $[\nu F_\nu]_{5\,\mathrm{GHz}}$ versus X-ray fluxes. Here, BLRGs are plotted as blue filled cycles when total radio fluxes are used, and

FIG. 7.— The dependence of the γ-ray luminosities (or upper limits for such), expressed in the Eddington units (L_γ/L_Edd) or as a ratio of the GeV and X-ray monochromatic luminosities (L_γ/L_X), on (i) the black hole mass $\mathcal{M}_\mathrm{BH}$ (*top left* panel), (ii) the accretion ratio $L_\mathrm{acc}/L_\mathrm{Edd}$ estimated from the SED fitting (*top right* panel), (iii) the proxy of the radio loudness parameter $L_\mathrm{R}/L_\mathrm{B}$ (*bottom left* panel), and (iv) the observed proxy of the accretion rate $L_\mathrm{B}/L_\mathrm{Edd}$ (*bottom right* panel). BLRGs and Seyferts are denoted by blue and red symbols, respectively. Large filled circles represent the two BLRGs detected by *Fermi*-LAT (3C 111 and 3C 120), while the medium-size open circles represent Pictor A. In the *bottom left* panel, when total radio

as cyan open circles when nuclear radio fluxes (obtained predominantly from VLBI observations where available, supplemented by VLA measurements in a few cases) are considered. In both panels, large symbols indicate the two objects detected by *Fermi*-LAT (3C 111 and 3C 120), while the medium-size symbols represent Pictor A galaxy which, even though not formally detected, is characterized by the third-highest TS in the analyzed two-year *Fermi*-LAT dataset. These flux-flux plots show that the optical and X-ray fluxes of BLRGs are roughly linearly correlated, as expected, though with a substantial (order-of magnitude) scatter. In addition, however, it is revealed that 3C 111, 3C 120, and also Pictor A, are at the same time the brightest in radio, but only when the nuclear (and not the total) radio fluxes are taken into account. Moreover, the nuclear radio fluxes seem well correlated with the X-ray fluxes for the whole BLRG population. Hence one may conclude that *Fermi*-LAT detects preferentially those BLRGs which are characterized by the brightest radio and X-ray nuclei. This supports the idea stated previously that the GeV emission of BLRGs is dominated by the innermost parts of their jets, and is therefore 'blazar-like,' being dependent on the jet luminosity and viewing angle. As argued above, the quasar 3C 273, for which the GeV luminosity is about 100 times higher than the nuclear radio luminosity, should provide a reasonably accurate template for such an emission. Indeed, as illustrated in Figure 6, the γ-ray–to–radio energy flux ratios for the two BLRGs detected by *Fermi*-LAT are of the order of $\simeq 100$, while the corresponding upper limits for all the other objects from the sample (including Seyferts) are above or much above this value. This indicates that the detections of BLRGs in γ rays are at present limited by the sensitivity of the *Fermi*-LAT instrument. In fact, from visual inspection of Figure 8 and 9, the predicted γ-ray flux from the template is very close to the *Fermi*-LAT upper limits for Pictor A, 3C 390.3, 3C 445, B3 0309+411B and PKS 2153-69.

Also it is important to note that the pc-scale components of the radio jets in both 3C 111 and 3C 120 are characterized by apparent superluminal motions with maximum velocities $\beta_{app} \simeq 5.9$ and 5.3, respectively, from MOJAVE monitoring data (Lister et al. 2009). The corresponding upper limits to the jet viewing angles are thus $\theta_j \lesssim 20°$. Interestingly, mildly relativistic velocities are inferred for 3C 390.3 and Pictor A (β_{app} up to $\simeq 2.2$ and 1.6, respectively; Kellermann et al. 2004; Tingay et al. 2000), both of which are good candidates for future *Fermi*-LAT detections (see Table 2 and Figure 8). These four BLRGs, not coincidentally, have the brightest radio/VLBI cores in the analyzed sample, consistent also with a relatively large degree of relativistic beaming (see the comment in Appendix A). Note also that 3C 303 and 3C 382 are other BLRGs with possible mildly relativistic pc-scale VLBI jets (Giovannini et al. 2001).

But what else — besides the nuclear radio jets — could be the source of high-energy emission in the considered objects? Clearly, large-scale structures (i.e., extended lobes, large-scale jets and terminal hotspots), which are particularly prominent in BLRGs, are expected to contribute *at least at some level* to the γ-ray emission in the GeV band, since the non-thermal synchrotron continua of these structures extend to the highest radio frequencies and even into the X-ray energies in some cases (see in this context *Fermi*-LAT detection of the extended lobes in the low-power radio galaxy Centaurus A; Abdo et al. 2010e). Such structures are on the other hand almost absent in Seyfert galaxies, due to much less prominent jet activity in those objects. Other possible

γ-ray emission sites in both BLRGs and Seyferts are their accretion disks and disk coronae. Several related (and rather preliminary) studies presented in the literature, even though not directly applicable to the types of astrophysical objects discussed here, indicate that other additional processes than those typically considered for generating high-energy photons within the accreting matter (e.g., proton-proton interactions), may be relevant in this context. In these scenarios, the resulting disk-related γ-ray emission may strongly depend on the main parameters of a black hole/accretion disk system (such as the black hole mass, spin, accretion rate, and disk inclination; see, e.g., Mahadevan et al. 1997; Oka & Manmoto 2003; Niedzwiecki et al. 2009). Hence it is interesting to look into this issue in more detail for all the sources included in our sample.

Figure 7 presents therefore the dependence of the γ-ray luminosities (or upper limits for such), expressed in the Eddington units (L_γ/L_{Edd}) or as a ratio of the GeV and X-ray monochromatic luminosities (L_γ/L_X), on (i) the black hole mass $\mathcal{M}_{BH}$ (*top left* panel), (ii) the accretion ratio L_{acc}/L_{Edd} determined from the model fitting (*top right* panel), (iii) the proxy of the radio loudness parameter L_R/L_B (*bottom left* panel), and (iv) the observed proxy of the accretion rate L_B/L_{Edd} (*bottom right* panel). In the figure, BLRGs and Seyferts are denoted by blue and red symbols, respectively. Large filled circles represent the two BLRGs detected by *Fermi*-LAT (3C 111 and 3C 120), while the medium-size open circles represent Pictor A. In the *bottom left* panel, when nuclear radio fluxes are used instead of the total radio fluxes, BLRGs are denoted by cyan symbols, and Seyferts by magenta symbols. A ratio of the GeV and X-ray monochromatic luminosities (L_γ/L_X) expected from a hybrid model is given as dashed lines in the *bottom right* panel, for different values of a mixing parameter $\eta = 10^{-2}$, 10^{-1}, and 1.

Note that the monochromatic luminosity ratio L_R/L_B is simply proportional to the 'standard' radio-loudness parameter $\mathcal{R}$, and in particular that $L_R/L_B = (\nu_R/\nu_B) \times \mathcal{R} \sim 10^{-5}\mathcal{R}$. Also, for the high accretion-rate objects analyzed in this paper one expects the accretion luminosity $L_{acc} \simeq L_{tot} \simeq 10 \times L_B$. As shown, the two galaxies which are the brightest in γ rays, and also Pictor A, are not characterized by any outstanding values of the radio loudness, accretion rate, or black hole mass, but are in fact quite representative for the other BLRGs included in the sample. This supports once again our conclusion that the detected GeV emission of BLRGs is related predominantly to nuclear jets, and not the other possible nuclear emission components. What should be noted for constraining theoretical models regarding the high-energy emission of accretion disks in AGN is the fact that, at least for a number of sources, the *Fermi*-LAT upper limits evaluated here already probe the GeV emission of BLRGs and Seyferts down to the levels of 1% of the X-ray (disk-related) luminosity, or equivalently 0.01% Eddington luminosity (see Figure 7).

APPENDIX

Here we present all the SEDs of the BLRGs (Figure 8) and Seyfert 1 galaxies (Figure 9) analyzed in this paper which are not detected by *Fermi*-LAT , together with the hybrid model fits described in the main text. The figures illustrate the expected level of the GeV emission of each source considered, in comparison with the current upper limits provided by two-years of *Fermi*-LAT data. Note in particular that the expected γ-ray fluxes of Pictor A, 3C 390.3 3C 445, B3 0309+411B and PKS 2153-69 are close to the *Fermi*-LAT limits derived in this paper (cf., Table 2). In contrast to the BLRGs (or at least the brightest and most beamed examples of such considered in this work), we speculate that the *jet-related* non-thermal emission of all the analyzed Seyfert 1 galaxies within the GeV photon energy range are in general beyond the level of detectability with *Fermi*-LAT .

REFERENCES

Abramowicz, M. A., Chen, X., Kato, S., Lasota, J.-P., & Regev, O. 1995, ApJ, 438, L37
Abdo, A. A., et al. 2009a, ApJ, 699, 31
Abdo, A. A., et al. 2009b, ApJ, 700, 597
Abdo, A. A., et al. 2009c, ApJ, 707, 55
Abdo, A. A., et al. 2009d, ApJ, 707, L142
Abdo, A. A., et al. 2010a, ApJ, 715, 429
Abdo, A. A., et al. 2010b, ApJS, 188, 405
Abdo, A. A., et al. 2010c, ApJ, 719, 1433
Abdo, A. A., et al. 2010d, ApJ, 720, 912
Abdo, A. A., et al. 2010e, Science, 328, 725
Aharonian, F., et al. 2008, A&A, 478, 387
Ajello, M., et al. 2008, ApJ, 673, 96
Ajello, M., et al. 2009, ApJ, 699, 603
Antonucci, R. 1993, ARA&A, 31, 473
Atwood, W. B., et al. 2009, ApJ, 697, 1071
Ballantyne, D. R., Fabian, A. C., & Iwasawa, K. 2004, MNRAS, 354, 839
Ballantyne, D. R. 2007, Modern Physics Letters A, 22, 2397
Barthel, P. D. 1989, ApJ, 336, 606
Beckmann, V., Gehrels, N., Shrader, C. R., & Soldi, S. 2006, ApJ, 638, 642
Bianchi, S., Matt, G., Haardt, F., Maraschi, L., Nicastro, F., Perola, G. C., Petrucci, P. O., & Piro, L. 2001, A&A, 376, 77
Bird, A. J., et al. 2007, ApJS, 170, 175
Blandford, R. D. 1990, in Active Galactic Nuclei, ed. T. J. -L. Courvoisier & M. Mayor (Berlin: Springer), 161
Blandford, R. D., & Znajek, R. L. 1977, MNRAS, 179, 433
Blustin, A. J., et al. 2003, A&A, 403, 481
Brenneman, L. W., Reynolds, C. S., Wilms, J., & Kaiser, M. E. 2007, ApJ, 666, 817
Brinkmann, W., Siebert, J., & Boller, T. 1994, A&A, 281, 355
Chatterjee, R., et al. 2011, ApJ, 734, 43
Courvoisier, T. J.-L. 1998, A&A Rev., 9, 1
Crawford, C. S., & Fabian, A. C. 1995, MNRAS, 273, 827
Dame, T. M., Hartmann, D., & Thaddeus, P. 2001, ApJ, 547, 792
Dasgupta, S., & Rao, A. R. 2006, ApJ, 651, L13
De Rosa, A., Piro, L., Fiore, F., Grandi, P., Maraschi, L., Matt, G., Nicastro, F., & Petrucci, P. O. 2002, A&A, 387, 838
De Rosa, A., Piro, L., Matt, G., & Perola, G. C. 2004, A&A, 413, 895
Dermer, C. D. 1995, ApJ, 446, L63
Donato, D., Sambruna, R. M., & Gliozzi, M. 2005, A&A, 433, 1163
Edelson, R. A. 1987, ApJ, 313, 651
Eracleous, M., & Halpern, J. P. 1994, ApJS, 90, 1
Eracleous, M., & Halpern, J. P. 1998, ApJ, 505, 577
Eracleous, M., & Halpern, J. P. 1994, ApJ, 599, 866
Eracleous, M., Sambruna, R., & Mushotzky, R. F. 2000, ApJ, 537, 654
Fabian, A. C., & Rees, M. J. 1995, MNRAS, 277, L55
Fomalont, E. B., Frey, S., Paragi, Z., Gurvits, L. I., Scott, W. K., Taylor, A. R., Edwards, P. G., & Hirabayashi, H. 2000, ApJS, 131, 95
Fukazawa, Y., et al. 2011, ApJ, 727, 19
Gallo, L. C. 2006, MNRAS, 368, 479
Garofalo, D. 2009, ApJ, 699, 400
Ghisellini, G., Tavecchio, F., & Chiaberge, M. 2005, A&A, 432, 401
Ghisellini, G., Maraschi, L., & Tavecchio, F. 2009, MNRAS, 396, L105
Giovannini, G., Feretti, L., & Comoretto, G. 1990, ApJ, 358, 159
Giovannini, G., Feretti, L., Venturi, T., Lara, L., Marcaide, J., Rioja, M., Spangler, S. R., & Wehrle, A. E. 1994, ApJ, 435, 116
Giovannini, G., Cotton, W. D., Feretti, L., Lara, L., Venturi, T. 2001, ApJ, 552, 508
Gliozzi, M., Sambruna, R. M., & Eracleous, M. 2003, ApJ, 584, 176
Gliozzi, M., Papadakis, I. E., Eracleous, M., Sambruna, R. M., Ballantyne, D. R., Braito, V., & Reeves, J. N. 2009, ApJ, 703, 1021
Gondoin, P., Lumb, D., Siddiqui, H., Guainazzi, M., & Schartel, N. 2001, A&A, 373, 805
Grandi, P., & Palumbo, G. G. C. 2004, Science, 306, 998
Grandi, P., & Palumbo, G. G. C. 2007, ApJ, 659, 235
Grandi, P., Urry, C. M., & Maraschi, L. 2002, New AR, 46, 221
Grandi, P., Malaguti, G., & Fiocchi, M. 2006, ApJ, 642, 113
Grandi, P., Guainazzi, M., Cappi, M., & Ponti, G. 2007, MNRAS, 381, L21
Hardcastle, M. J., Croston, J. H., & Kraft, R. P. 2007, ApJ, 669, 893
Hartman, R. C., Kadler, M., & Tueller, J. 2008, ApJ, 688, 852
Henstock, D. R., Browne, I. W. A., Wilkinson, P. N., Taylor, G. B., Vermeulen, R. C., Pearson, T. J., & Readhead, A. C. S. 1995, ApJS, 100, 1
Hewitt, A., & Burbidge, G. 1991, ApJS, 75, 297
Hirabayashi, H., et al. 2000, PASJ, 52, 997
Ho, L. C. 2002, ApJ, 564, 120
Ho, L. C., & Peng, C. Y. 2001, ApJ, 555, 650
Ho, L. C., Ptak, A., Terashima, Y., Kunieda, H., Serlemitsos, P. J., Yaqoob, T., & Koratkar, A. P. 1999, ApJ, 525, 168
Hough, D. H., Vermeulen, R. C., Readhead, A. C. S., Cross, L. L., Barth, E. L., Yu, L. H., Beyer, P. J., & Phifer, E. M. 2002, AJ, 123, 1258
Inoue, H., Terashima, Y., & Ho, L. C. 2007, ApJ, 662, 860
Inoue, Y., Totani, T., & Ueda, Y. 2008, ApJ, 672, L5
Kaspi, S., Maoz, D., Netzer, H., Peterson, B. M., Vestergaard, M., & Jannuzi, B. T. 2005, ApJ, 629, 61
Kataoka, J., Edwards, P., Georganopoulos, M., Takahara, F., & Wagner, S. 2003, A&A, 399, 91
Kataoka, J., et al. 2007, PASJ, 59, 279
Kataoka, J., et al. 2010, ApJ, 715, 554
Kellermann, K. I., Sramek, R., Schmidt, M., Shaffer, D. B., & Green, R. 1989, AJ, 98, 1195
Kellermann, K. I., et al. 2004, ApJ, 609, 539
Koide, S., Shibata, K., Kudoh, T., & Meier, D. L. 2002, Science, 295, 1688
Komatsu, E., et al. 2009, ApJS, 180, 330
Komossa, S. 2008, Revista Mexicana de Astronomia y Astrofisica Conference Series, 32, 86
Koratkar, A., & Blaes, O. 1999, PASP, 111, 1
Kukula, M. J., Pedlar, A., Baum, S. A., & O'Dea, C. P. 1995, MNRAS, 276, 1262

Labita, M., Treves, A., Falomo, R., & Uslenghi, M. 2006, MNRAS, 373, 551

Larsson, J., Miniutti, G., Fabian, A. C., Miller, J. M., Reynolds, C. S., & Ponti, G. 2008, MNRAS, 384, 1316

Laurent-Muehleisen, S. A., Kollgaard, R. I., Ryan, P. J., Feigelson, E. D., Brinkmann, W., & Siebert, J. 1997, A&AS, 122, 235

Lasota, J.-P. 1996, Basic Physics of Accretion Disks, 85

Lewis, K. T., Eracleous, M., Gliozzi, M., Sambruna, R. M., & Mushotzky, R. F. 2005, ApJ, 622, 816

Linfield, R. 1987, ApJ, 317, 121

Lister, M. L. et al., 2009, ApJ, 138, 1874

Liu, Y., Jiang, D. R., & Gu, M. F. 2006, ApJ, 637, 669

Mahadevan, R., Narayan, R., & Krolik, J. 1997, ApJ, 486, 268

Maraschi, L., Chiappetti, L., Falomo, R., Garilli, B., Malkan, M., Tagliaferri, G., Tanzi, E. G., & Treves, A. 1991, ApJ, 368, 138

Marchesini, D., Celotti, A., & Ferrarese, L. 2004, MNRAS, 351, 733

Markowitz, A. G., & Reeves, J. N. 2009, ApJ, 705, 496

Mattox, J. R., et al. 1996, ApJ, 461, 396

Middelberg, E., et al. 2004, A&A, 417, 925

Molina, M., et al. 2008, MNRAS, 390, 1217

Molina, M., et al. 2009, MNRAS, 399, 1293

Nandra, K., O'Neill, P. M., George, I. M., & Reeves, J. N. 2007, MNRAS, 382, 194

Narayan, R., & Yi, I. 1994, ApJ, 428, L13

Narayan, R., & Yi, I. 1995, ApJ, 444, 231

Neff, S. G., Roberts, L., & Hutchings, J. B. 1995, ApJS, 99, 349

Niedzwiecki, A., Xie, F. G., & Zdziarski, A. A. 2009, Proceedings of "The Extreme Sky: Sampling the Universe above 10 keV"

O'Dea, C. P. 1998, PASP, 110, 493

Oka, K., & Manmoto, T. 2003, MNRAS, 340, 543

Ogle, P. M., Davis, S. W., Antonucci, R. R. J., Colbert, J. W., Malkan, M. A., Page, M. J., Sasseen, T. P., & Tornikoski, M. 2005, ApJ, 618, 139

O'Neill, P. M., Nandra, K., Cappi, M., Longinotti, A. L., & Sim, S. A. 2007, MNRAS, 381, L94

Pearson, T. J., Blundell, K. M., Riley, J. M., & Warner, P. J. 1992, MNRAS, 259, 13

Perley, R. A., Roser, H.-J., & Meisenheimer, K. 1997, A&A, 328, 12

Pogge, R. W., 2000, New AR, 44, 381

Preuss, E., & Fosbury, R. A. E. 1983, MNRAS, 204, 783

Reeves, J. N., & Turner, M. J. L. 2000, MNRAS, 316, 234

Reynolds, C. S., Brenneman, L. W., Wilms, J., & Kaiser, M. E. 2004, MNRAS, 352, 205

Sambruna, R. M., George, I. M., Mushotzky, R. F., Nandra, K., & Turner, T. J. 1998, ApJ, 495, 749

Sambruna, R. M., Eracleous, M., & Mushotzky, R. F. 1999, ApJ, 526, 60

Sambruna, R. M., Eracleous, M., & Mushotzky, R. F. 2002, New AR, 46, 215

Sambruna, R. M., Reeves, J. N., & Braito, V. 2007, ApJ, 665, 1030

Sambruna, R. M., et al. 2009, ApJ, 700, 1473

Sambruna, R. M., Tombesi, F., Reeves, J. N., Braito, V., Ballo, L., Gliozzi, M., & Reynolds, C. S. 2011, ApJ, 734, 105

Sazonov, S., Revnivtsev, M., Krivonos, R., Churazov, E., & Sunyaev, R. 2007, A&A, 462, 57

Schlegel, D. J., Finkbeiner, D. P., & Davis, M. 1998, ApJ, 500, 525

Schmoll, S., et al. 2009, ApJ, 703, 2171

Shakura, N. I., & Sunyaev, R. A. 1973, A&A, 24, 337

Shinozaki, K., Miyaji, T., Ishisaki, Y., Ueda, Y., & Ogasaka, Y. 2006, AJ, 131, 2843

Sikora, M., Begelman, M. C., & Rees, M. J. 1994, ApJ, 421, 153

Sikora, M., Stawarz, Ł., & Lasota, J.-P. 2007, ApJ, 658, 815

Soldi, S., et al. 2008, A&A, 486, 411

Steenbrugge, K. C., Kaastra, J. S., Sako, M., Branduardi-Raymont, G., Behar, E., Paerels, F. B. S., Blustin, A. J., & Kahn, S. M. 2005, A&A, 432, 453

Taylor, G. B., Vermeulen, R. C., Readhead, A. C. S., Pearson, T. J., Henstock, D. R., & Wilkinson, P. N. 1996, ApJS, 107, 37

Tchekhovskoy, A., Narayan, R., & McKinney, J. C. 2010, ApJ, 711, 50

Thean, A. H. C., Gillibrand, T. I., Pedlar, A., & Kukula, M. J. 2001, MNRAS, 327, 369

Tingay, S. J., et al. 2000, AJ, 119, 1695

Tazaki, F., Ueda, Y., Ishino, Y., Eguchi, S., Isobe, N., Terashima, Y., & Mushotzky, R. F. 2010, ApJ, 721, 1340

Tingay, S. J., et al. 2002, ApJS, 141, 311

Tingay, S. J., Jauncey, D. L., King, E. A., Tzioumis, A. K., Lovell, J. E. J., & Edwards, P. G. 2003, PASJ, 55, 351

Tueller, J., et al. 2010, ApJS, 186, 378

Turner, T. J., & Pounds, K. A. 1989, MNRAS, 240, 833

Ulvestad, J. S., & Wilson, A. S. 1989, ApJ, 343, 659

Urry, C. M., & Padovani, P. 1995, PASP, 107, 803

Veron-Cetty, M. P., Woltjer, L., & Roy, A. L. 1991, A&A, 246, L73

Wang, J., Mao, Y. F., & Wei, J. Y. 2009, AJ, 137, 3388

White, R. L., et al. 2000, ApJS, 126, 133

Wozniak, P. R., Zdziarski, A. A., Smith, D., Madejski, G. M., & Johnson, W. N. 1998, MNRAS, 299, 449

Young, A. J., Wilson, A. S., Tingay, S. J., & Heinz, S. 2005, ApJ, 622, 830

Zdziarski, A. A., & Grandi, P. 2001, ApJ, 551, 186

Zhou, X.-L., Zhang, S.-N., Wang, D.-X., & Zhu, L. 2010, ApJ, 710, 16

TABLE 1
MULTIWAVELENGTH PROPERTIES OF THE ANALYZED BLRGS AND SEYFERTS

IAU J2000	name	z	$d_{\rm L}$ [Mpc]	$[\nu F_\nu]^{\rm tot}_{\rm 5\,GHz}$ $\times 10^{-14}$ [erg/cm^2/s]	$[\nu F_\nu]^{\rm nuc}_{\rm 5\,GHz}$ $\times 10^{-14}$ [erg/cm^2/s]	$[\nu F_\nu]^{\rm nuc}_{\rm B}$ $\times 10^{-12}$ [erg/cm^2/s]	$\Gamma_{\rm X}$	$[\nu F_\nu]_{\rm 2-10\,keV}$ $\times 10^{-12}$ [erg/cm^2/s]	$[\nu F_\nu]_{\rm 14-195\,keV}$ $\times 10^{-12}$ [erg/cm^2/s]	$\log M_{\rm BH}$ [$M_\odot$]	References[a]
BLRGs											
0040+1003	3C 18	0.188	833.4	9.2	0.31	1.4	1.9	2.6	–	8.92	1-5
0313+4120	B3 0309+411B	0.134	608.1	2.5	1.6	2.2	1.9	9.0	–	–	6-9
0418+3801	3C 111	0.0485	207.1	39	8.5	193	1.7	37	141	8.80	1,6-7,10-16,25
0433+0521	3C 120	0.033	139.3	26	19	82	1.9	62	119	7.75	1,10-13,17-24
0519-4546	Pictor A	0.0351	148.4	77	3.8	6.8	1.7	16	38	8.70	1,11−13,16,22−25
0906+1646	3C 215	0.412	2183	2.1	0.082	1.5	1.7	2.3	–	8.80	11,29−31
0947+0725	3C 227	0.0858	376.6	13	0.11	6.2	1.5f	1.0[b]	27	8.90	13,32−35
1443+5201	3C 303	0.141	642.9	4.7	0.75	0.7	1.9	2.0	–	8.00	11,25,35,36
1722+2436	RGB J1722+246	0.175	815.6	0.17	0.14	7.1	1.8	1.0	–	–	1,3,37
1835+3241	3C 382	0.0579	249.0	11	0.94	17	1.7	46	84	8.90	1,9−13,22,25,38,39
1842+7946	3C 390.3	0.0561	240.9	22	2.0	31	1.7	34	110	8.80	1,6,7,9−11,13,17, 19,20,22,25,40,41
2022+1001	3C 411	0.467	2536	4.5	0.39	0.6	1.8	0.8	–	–	2,11,31,75
2042+7508	4C 74.26	0.104	462.4	1.7	0.5	74	1.8	20	50	9.37	6,7,9,13,22,42,43
2114+8204	S5 2116+81	0.084	368.2	1.2	0.49	17	1.9	15	42	8.12	1,6,7,9,13,43,44
2124+5058	4C 50.55	0.020	83.6	5.0	1.0[d]	–[c]	1.4	51	178	–	6,7,9,13,45
2157-6941	PKS 2153-69	0.0283	119	60	1.5	44	1.8	7.2	–	–	1,46,47
2223-0206	3C 445	0.0562	241.4	10	0.41	2.9	1.6	15	44	8.00	1,9−11,13,22, 25,48−51
2254+1136	PKS 2251+11	0.326	1656	3.0	0.01	11	1.1	1.5	–	8.93	11,31,52,53
Seyferts											
0006+2012	Mrk 335	0.0258	114.2	0.016	0.016	5.1	2.0	13.5	24.7	6.80	13,22,25,54−60,76
0123-5848	Fairall 9	0.047	214.1	<0.025	<0.025	145	1.7	20.5	50.7	7.90	13,22,25,54,61−63,76,77
0516-0008	Ark 120	0.0327	144.2	0.062	0.015	201	2.2	32.5	70.8	8.30	13,22,25,54,64,65,76
0925+5217	Mrk 110	0.0353	158.3	0.027	0.011	8.4	1.7	28.0	61.5	6.70	13,22,25,54,64−66,76
1139-3744	NGC 3783	0.00973	38.5	0.12	0.065	89	1.6	49.0	195	7.00	9,13,22,25,54, 61,64,67,76
1239-0520	NGC 4593	0.009	39.5	0.013	0.0081	27	1.8	36.5	97.9	6.90	13,22,25,54,68−71,76
1349-3018	IC4329A	0.0161	70.2	0.18	0.17	34	1.7	90.0	331	6.70	9,22,25,54,61,64,72,76
2044-1043	Mrk 509	0.0344	154.1	0.051	0.026	140	1.6	44.0	94.4	7.80	9,22,25,54,61,68,71,76
2303+0852	NGC 7469	0.0163	71.4	0.39	0.30	10	1.8	31.5	66.6	6.80	9,25,54,61,64,74,76

[a] References: [1] Grandi et al. (2006); [2] Hewitt & Burbidge (1991); [3] Laurent-Muehleisen et al. (1997); [4] Marchesini et al. (2004); [5] Brinkmann et al. (1994); [6] Molina et al. (2008); [7] Molina et al. (2009); [8] Henstock et al. (1995); [9] Bird et al. (2007); [10] Wozniak et al. (1998); [11] Sambruna et al. (1999); [12] Eracleous et al. (2000); [13] Tueller et al. (2010); [14] Turner & Pounds (1989); [15] Linfield (1987); [16] Lewis et al. (2005); [17] Gliozzi et al. (2003); [18] Kataoka et al. (2007); [19] Hirabayashi et al. (2000); [20] Fomalont et al. (2000); [21] Zhou et al. (2010); [22] Fukazawa et al. (2011); [23] Ogle et al. (2005); [24] Ballantyne et al. (2004); [25] Sikora et al. (2007); [26] Tingay et al. (2003); [27] Tingay et al. (2000); [28] Eracleous & Halpern (1998); [29] Hough et al. (2002); [30] Labita et al. (2006); [31] Reeves & Turner (2000); [32] Crawford & Fabian (1995); [33] Hardcastle et al. (2007); [34] Ajello et al. (2008); [35] Kataoka et al. (2003); [36] Giovannini et al. (1990); [37] Donato et al. (2005); [38] Giovannini et al. (1994); [39] Sambruna et al. (2011); [40] Gliozzi et al. (2009); [41] Sambruna et al. (2009); [42] Pearson et al. (1992); [43] Wang et al. (2009); [44] Taylor et al. (1996); [45] Tazaki et al. (2010); [46] Tingay et al. (2002); [47] Young et al. (2005); [48] Preuss & Fosbury (1983); [49] Grandi et al. (2007); [50] Sambruna et al. (2007); [51] Sambruna et al. (1998); [52] Kellermann et al. (1989); [53] Liu et al. (2006); [54] Kaspi et al. (2005); [55] Edelson (1987); [56] Gallo (2006); [57] Inoue et al. (2007); [58] Larsson et al. (2008); [59] Bianchi et al. (2001); [60] O'Neill et al. (2007); [61] Shinozaki et al. (2006); [62] Schmoll et al. (2009); [63] Gondoin et al. (2001); [64] Nandra et al. (2007); [65] Sazonov et al. (2007); [66] Dasgupta & Rao (2006); [67] De Rosa et al. (2002); [66] Beckmann et al. (2006); [69] Reynolds et al. (2004); [70] Brenneman et al. (2007); [71] Markowitz & Reeves (2009); [72] Steenbrugge et al. (2005); [73] De Rosa et al. (2004); [74] Blustin et al. (2003); [75] Neff et al. (1995); [76] Ho (2002); [77] Veron-Cetty et al. (1991).

[b] Flux estimated from the counts rate of *Chandra* ACIS CCD chip using PIMMS and assuming the X-ray photon index $\Gamma_{\rm X} = 1.5$.

[c] Unreliable extinction estimate due to the location of the source at low Galactic latitude $|b| < 5$ deg.

[d] 5 GHz flux was obtained from our new VLBA observations obtained on 2009 Feb 7 in program BC 185 (PI: C. C. Cheung).

TABLE 2
RESULTS OF THE *Fermi*-LAT DATA ANALYSIS

name	TS	Γ_γ	$F_{>0.1\,\mathrm{GeV}}$ $[10^{-9}\,\mathrm{ph\,cm^{-2}\,s^{-1}}]$	$[\nu F_\nu]_{0.1-10\,\mathrm{GeV}}$ $[10^{-12}\,\mathrm{erg\,cm^{-2}\,s^{-1}}]$	$\log L_\gamma$ $[\mathrm{erg\,s^{-1}}]$	$\log L_{\mathrm{acc}}$[a] $[\mathrm{erg\,s^{-1}}]$	η[b]
BLRGs							
3C 18	1.5	2.5f[c]	< 9.2	< 4.0	< 44.6	45.3	0.070
B3 0309+411B	< 1	2.5f	< 8.9	< 3.9	< 44.3	45.5	0.12
3C 111	31	2.7±0.2	35±12	15	43.9	45.0	0.35
3C 120	34	3.0±0.3	37±14	16	43.6	44.9	0.15
Pictor A	20	2.5f	< 15	< 6.3	< 43.2	44.5	0.25
3C 215	13	2.5f	< 14	< 6.1	< 45.6	45.9	0.034
3C 227	< 1	2.5f	< 5.0	< 2.2	< 43.6	44.9	0.017
3C 303	2.0	2.5f	< 5.9	< 2.6	< 44.1	45.0	0.20
RGB J1722+246	< 1	2.5f	< 38	< 16	< 45.1	45.0	0.058
3C 382	2.8	2.5f	< 12	< 5.2	< 43.6	45.1	0.025
3C 390.3	3.2	2.5f	< 7.4	< 3.2	< 43.4	45.0	0.075
3C 411	8.4	2.5f	< 18	< 7.6	< 45.8	45.7	0.17
4C 74.26	3.1	2.5f	< 11	< 4.7	< 44.1	45.6	0.015
S5 2116+81	1.6	2.5f	< 5.9	< 2.6	< 43.6	45.3	0.023
4C 50.55	< 1	2.5f	< 180	< 77	< 43.8	44.4	0.024
PKS 2153-69	1.4[d]	2.5f	< 10	< 4.4	< 42.9	44.2	0.10
3C 445	< 1	2.5f	< 2.1	< 0.90	< 42.8	44.8	0.022
PKS 2251+11	< 1	2.5f	< 5.4	< 2.3	< 44.9	45.4	0.010
Seyferts							
Mrk 335	8.9	2.5f	< 11	< 4.8	< 42.9	44.6	2.6×10^{-4}
Fairall 9	< 1	2.5f	< 1.9	< 0.81	< 42.6	45.0	$< 4.0\times10^{-4}$
Ark 120	< 1	2.5f	< 2.8	< 1.2	< 42.5	44.9	2.3×10^{-4}
Mrk 110	3.9	2.5f	< 6.9	< 3.0	< 42.9	44.8	3.3×10^{-4}
NGC 3783	< 1	2.5f	< 3.2	< 1.4	< 41.5	44.1	4.6×10^{-4}
NGC 4593	2.5	2.5f	< 8.9	< 3.9	< 41.8	43.9	1.3×10^{-4}
IC4329A	15	2.5f	< 19	< 8.1	< 42.7	44.7	1.0×10^{-3}
Mrk 509	< 1	2.5f	< 2.7	< 1.2	< 42.5	45.1	3.2×10^{-4}
NGC 7469	< 1	2.5f	< 7.1	< 3.1	< 42.3	44.8	1.2×10^{-3}

[a] Accretion luminosity derived from the SED fitting, assuming hybrid model discussed in the paper.

[b] Mixing parameter described in the text, derived from the SED fitting.

[c] Photon spectral index was fixed at 2.5.

[d] A nearby LAT source was found 0.27 deg apart from PKS 2153-69 with TS of 44. We treat this as a background source since its separation from the target is more than 2 times larger than its 95 % γ-ray localization error radius.
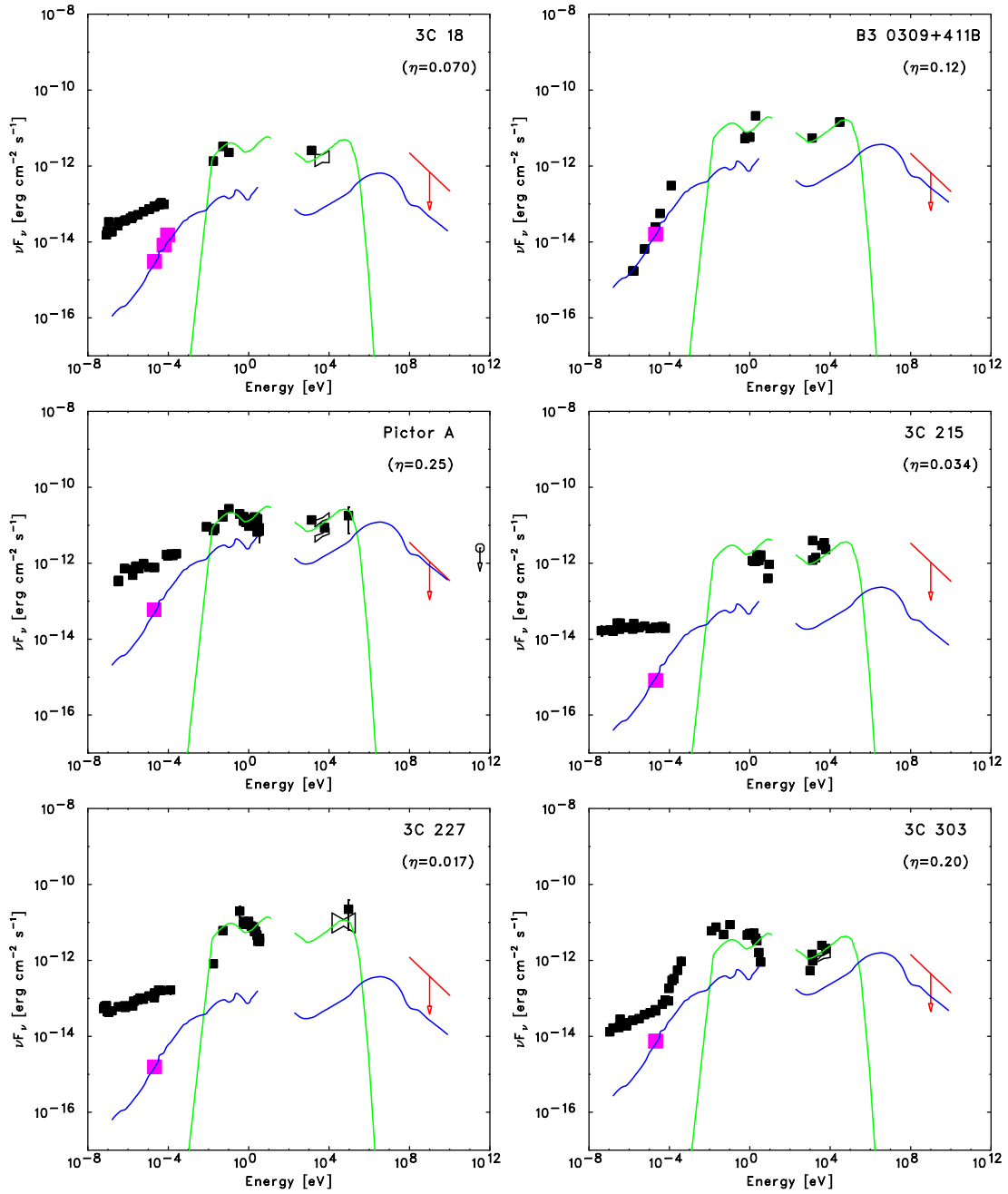
FIG. 8.— Broad-band SEDs of the BLRGs which are *not* detected at high significance in the GeV photon energy range. *Fermi*-LAT upper limits are indicated by red arrows. Black squares represent the historical data from NED. Magenta squares denote the 5 GHz radio fluxes of the unresolved nuclei. The green curves correspond to the template of the accretion-related Seyfert-type emission (from Koratkar & Blaes 1999), matched to the infrared–to–X-ray continuum of each source. The blue curves correspond to the broad-band spectrum of the quasar 3C 273 (from Soldi et al. 2008), used here as a template of the jet-related emission and scaled to match the radio fluxes for each source. The mixing parameter η for the phenomenological hybrid model discussed in § 4 is given in each panel.
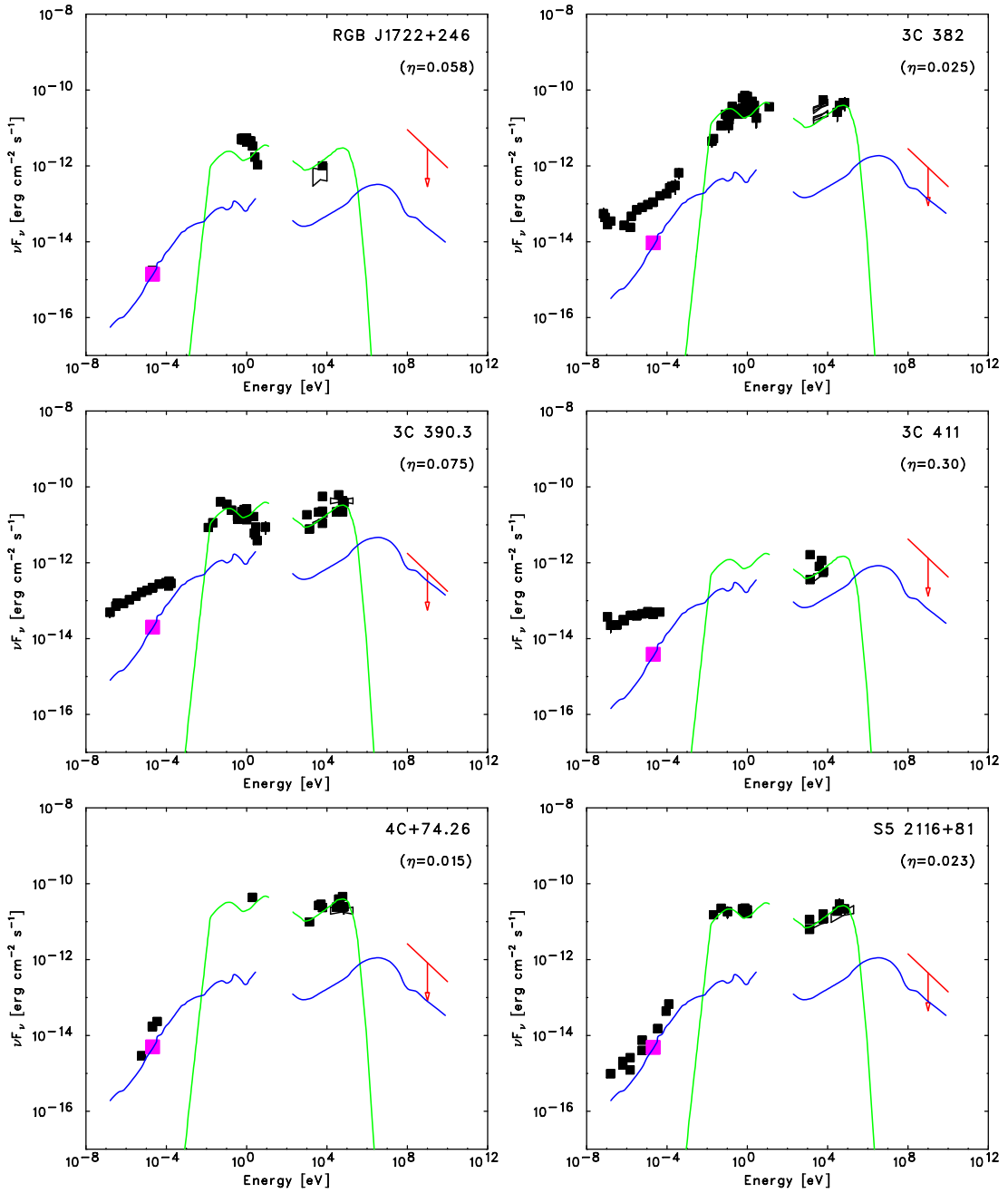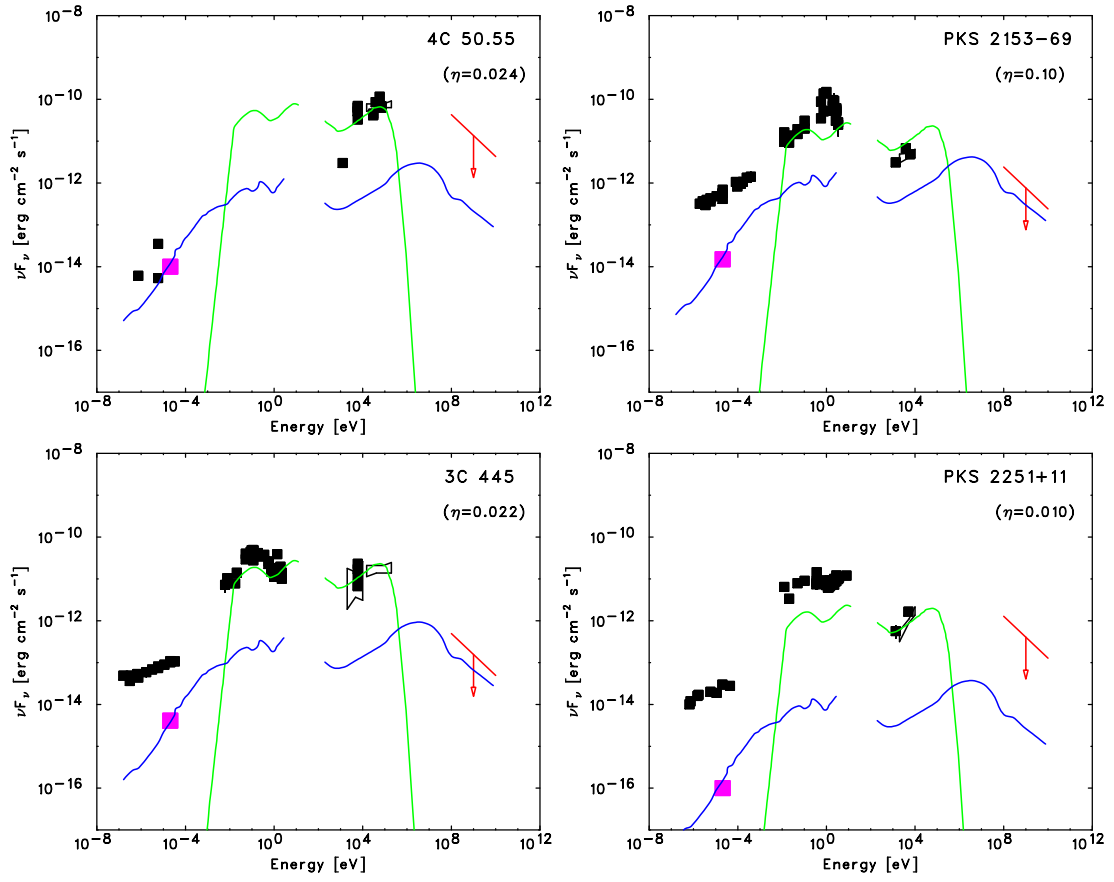
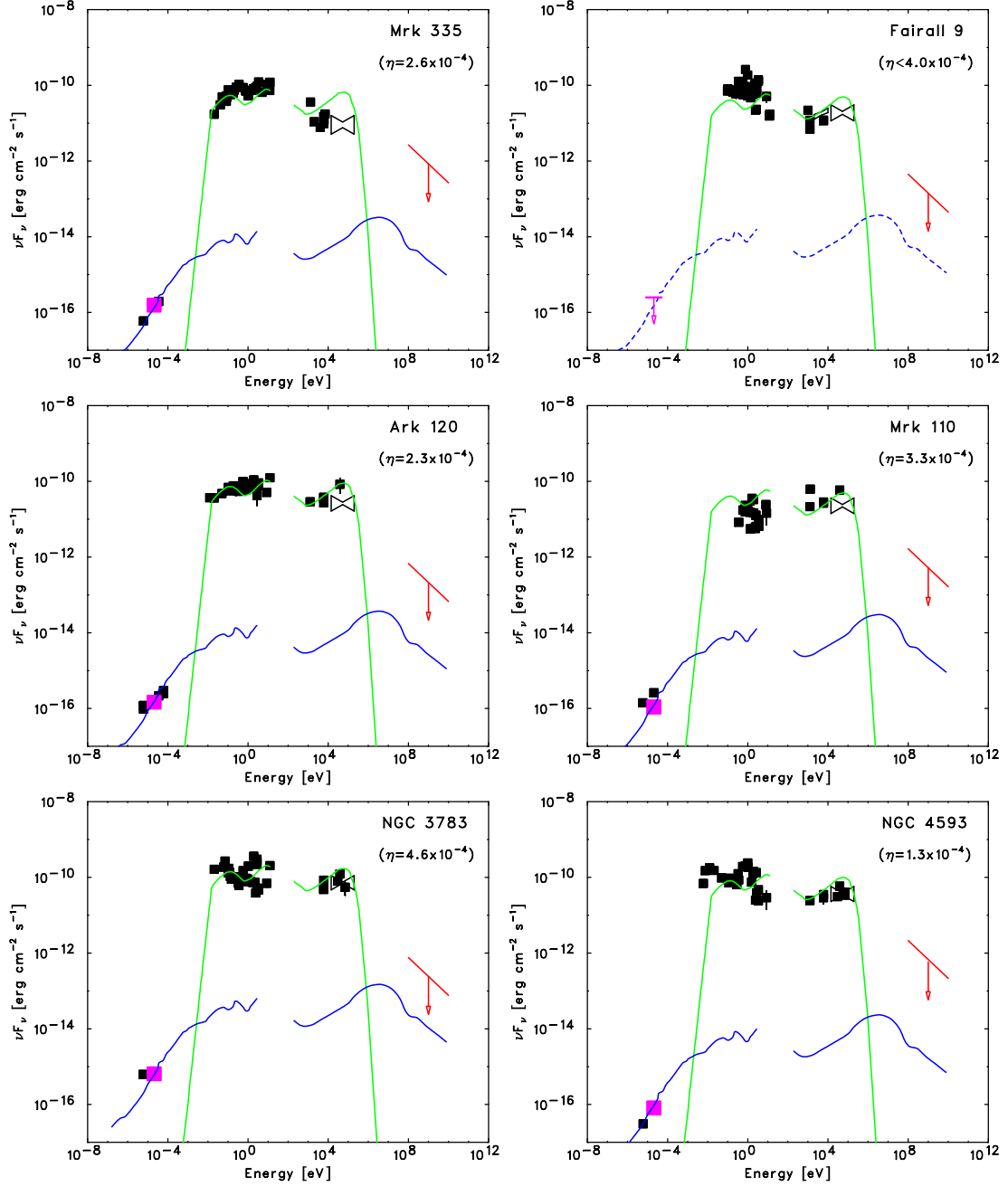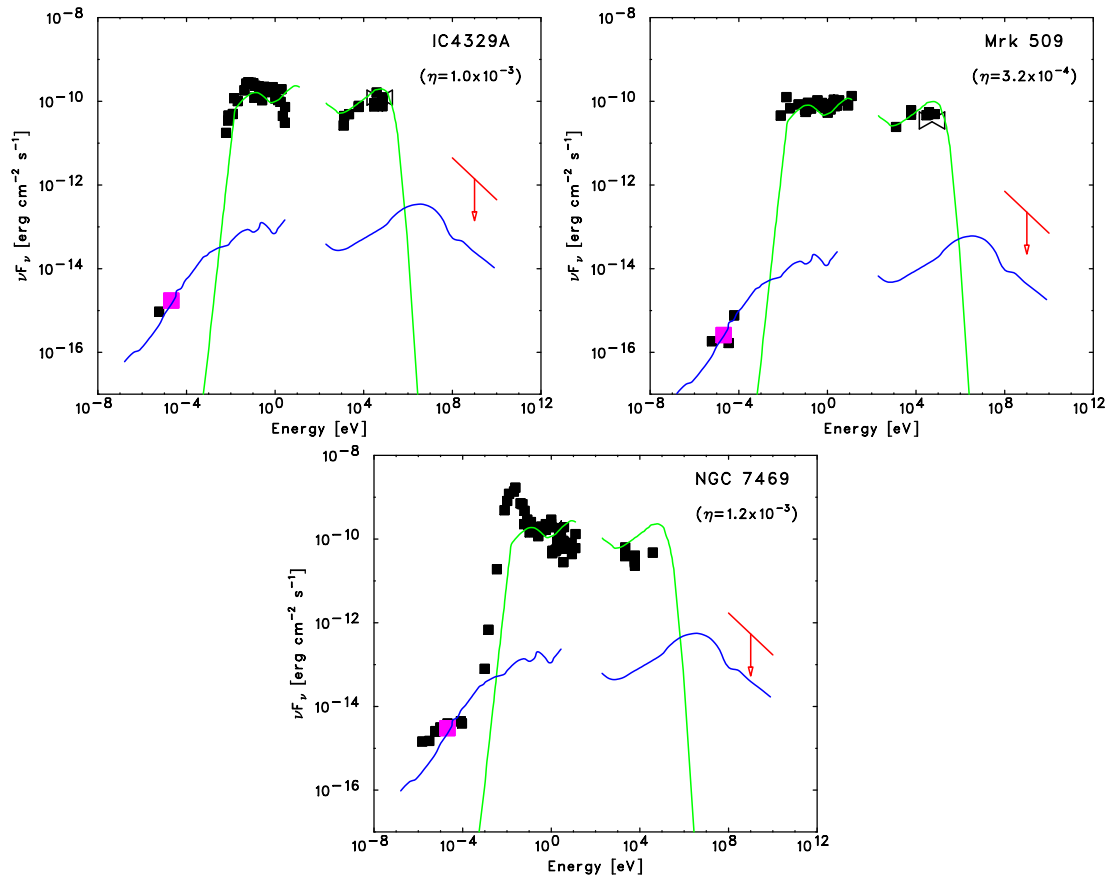FIG. 8.— —*continued.*

FIG. 8.— —continued.

Fig. 9.— Broad-band SEDs of the high-accretion Seyfert 1 galaxies. *Fermi*-LAT upper limits are indicated by red arrows. Black squares represent the historical data from NED. Magenta squares denote the 5 GHz radio fluxes of the unresolved nuclei, except for Fairall 9 where a radio detection has not been reported in the literature. The green curves correspond to the template of the accretion-related Seyfert-type emission (from Koratkar & Blaes 1999), matched to the infrared–to–X-ray continuum of each source. The blue curves correspond to the broad-band spectrum of the quasar 3C 273 (from Soldi et al. 2008), used here as a template of the jet-related emission and scaled to match the radio fluxes for each source. The mixing parameter η for the phenomenological hybrid model discussed in §4 is given in each panel.

Kataoka et al.

FIG. 9.— —*continued.*